# A kinetochore-centrosome feedback loop linking CENP-E and Aurora kinases controls chromosome biorientation and congression

Kruno Vukušić*, Iva M. Tolić*

Division of Molecular Biology, Ruđer Bošković Institute, Zagreb, Croatia

*Corresponding authors

E-mail: kvukusic@irb.hr, tolic@irb.hr

**ABSTRACT**

Chromosome congression to the spindle equator is crucial for accurate cell division, as its failure leads to aneuploidy. The kinetochore motor protein CENP-E/kinesin-7 is uniquely required for congression of chromosomes near centrosomes, yet the reasons for this dependency are unclear. Current models suggest that CENP-E drives congression by gliding kinetochores along microtubules. Here, we propose an alternative model wherein CENP-E initiates chromosome movement by promoting the formation of end-on attachments on kinetochores rather than directly propelling them. Our live-cell and super-resolution imaging under varying CENP-E activity shows that without CENP-E, congression is delayed due to Aurora A-mediated activation of Aurora B near centrosomes. This activation limits biorientation by increasing the phosphorylation of microtubule-binding proteins on kinetochores and promoting the expansion of the fibrous corona. CENP-E counters this inhibition by reducing Aurora B-mediated phosphorylation of outer-kinetochore proteins in a BuBR1-dependent manner, thereby stabilizing end-on attachments, leading to removal of the fibrous corona and initiation of chromosome movement. Without CENP-E, cancer cells cannot align polar chromosomes after a certain time point, highlighting a mitotic timing-dependent vulnerability in cancers.

Keywords: Mitosis/Chromosome congression/Kinetochore/Aurora kinases/Centrosome/CENP-E

## INTRODUCTION

To ensure equal segregation into the two daughter cells, duplicated chromosomes achieve biorientation by attaching to microtubules extending from opposite spindle poles, thereby satisfying the spindle assembly checkpoint (SAC) (Maiato *et al*, 2017; McAinsh & Kops, 2023; Valdez *et al*, 2023). During early mitosis, chromosomes exhibit characteristic movement towards the equatorial region of the spindle, a process known as chromosome congression (Barisic *et al*, 2014). Chromosomes positioned near spindle poles, referred to as polar chromosomes, require the activity of the kinetochore motor protein CENtromere-associated Protein-E (CENP-E/kinesin-7) for congression (Barisic *et al*, 2014). Polar chromosomes are particularly prone to alignment failure during shortened mitosis in healthy and unperturbed mitosis in cancer cells (Gomes *et al*, 2022; Tucker *et al*, 2023; Klaasen *et al*, 2022). Consequently, congression of polar chromosomes appears to exhibit distinct dynamics, signaling mechanisms, and final efficiency (Vukušić & Tolić, 2022).

CENP-E function in chromosome movement has been studied extensively (Yen *et al*, 1992, 1991; Weaver *et al*, 2003; Schaar *et al*, 1997; Mao *et al*, 2005; Kapoor *et al*, 2006; Kim *et al*, 2008; Gudimchuk *et al*, 2013; Yao *et al*, 1997; Shrestha & Draviam, 2013; Bancroft *et al*, 2015; Barisic *et al*, 2014; Maiato *et al*, 2017; Auckland & McAinsh, 2015). The prevailing model states that CENP-E glides polar kinetochores that are attached laterally to microtubules towards equatorial plate independently of chromosome biorientation, utilizing its microtubule plus-end directed motor activity (Kapoor *et al*, 2000; Cai *et al*, 2009; Walczak *et al*, 2010). The preference for CENP-E in a tug of war with the minus-end directed kinetochore motor dynein is facilitated by a single-site (T422) phosphorylation of CENP-E by Aurora kinases close to the spindle poles (Kim *et al*, 2010) and by tubulin detyrosination of kinetochore fibers (Barisic *et al*, 2015), both of which enhance CENP-E activity (Barisic & Maiato, 2015; Kops & Gassmann, 2020). CENP-E is recruited to an unattached outer kinetochore by BuBR1 (Cmentowski *et al*, 2023), and to a fibrous corona (Cooke *et al*, 1997) by the Rod-Zw10-Zwilch (RZZ) complex and Dynein-Dynactin (Weber *et al*, 2024; Cmentowski *et al*, 2023), which sheds from the kinetochore upon stable end-on attachment formation (Yen *et al*, 1991; Kops & Gassmann, 2020). However, despite the established requirement of CENP-E for chromosome congression, polar chromosomes initially move towards the spindle equator without CENP-E activity but eventually fail to align (Renda *et al*, 2022). Moreover, congression occurs after delays even in complete absence of CENP-E (Kim *et al*, 2010; Maia *et al*, 2010; Barisic *et al*, 2014; Bancroft *et al*, 2015; Iemura & Tanaka, 2015), contradicting the prevailing model. Thus, the mechanism of chromosome congression and the precise function of CENP-E in this process remain unclear.

Here, we reveal that chromosome congression involves two distinct mechanical steps: initiation and movement. CENP-E plays a critical role in initiating congression by facilitating the formation of end-on attachments rather than directly driving chromosome movement. This finding challenges the current model (Kapoor *et al*, 2006), but aligns with pioneering models emphasizing the requirement for biorientation in congression (McEwen *et al*, 1997). Our discovery agrees with previous work demonstrating the involvement of CENP-E in lateral to end-on conversion (Shrestha & Draviam, 2013). However, instead of maintaining lateral attachment, we propose that

CENP-E is involved in the establishment or stabilization of end-on attachments. We arrived at this conclusion by developing a large-scale live-cell imaging strategy using lattice light-sheet microscopy (LLSM), which allowed us to observe numerous chromosome congression events across many cells simultaneously. Combined with reversible chemical inhibition experiments targeting key molecules implicated in congression, we resolved the hierarchical molecular networks underlying this process over space and time. Our data demonstrate that CENP-E initiates the stabilization of end-on attachments—a crucial initial step in congression preceding chromosome movement—marked by a gradual decrease in SAC proteins and concurrent formation of end-on attachments observed via super-resolution microscopy. We uncovered a negative feedback loop involving Aurora B kinase, which counters congression by destabilizing end-on attachments near the spindle pole following activation by Aurora A in the proximity of centrosomes. Interestingly, Aurora kinases also activate CENP-E (Kim *et al*, 2010), suggesting a complex interplay where CENP-E, in a BubR1-dependent manner, counteracts the combined activity of Aurora kinases to promote congression. Furthermore, our study reveals that in the absence of CENP-E, excessive expansion of the fibrous corona also impedes the formation of end-on attachments and chromosome congression—a barrier relieved by Aurora B kinase inhibition. Finally, we demonstrate that without CENP-E, chromosomally unstable cancer cells are less efficient in initiating congression during prolonged mitosis compared to non-cancer cells, highlighting the crucial role of CENP-E in maintaining mitotic fidelity, especially in cancer contexts. These findings underscore the sensitivity of chromosomally unstable cancers to congression defects and SAC activation (Quinton *et al*, 2021), suggesting differential responses to prolonged mitosis between healthy and cancer cells.

## RESULTS

### CENP-E is essential only for the initiation of movement during chromosome congression

To untangle the complex molecular mechanisms of chromosome congression (Maiato *et al*, 2017), we developed an assay to systematically test the roles of specific molecular players. By usage of CENP-E inactivation or depletion, referred to jointly as CENP-E perturbation, we created two distinct populations of chromosomes—those aligned at the spindle midplane and polar chromosomes—resulting in mitotic spindles with synchronized chromosomes near the spindle poles. This approach minimizes the variabilities between chromosomes typically observed in unperturbed mitosis (Magidson *et al*, 2011). To simultaneously image many individual cells (1.5 mm field of view) in complete volumes (35 μm depth) with high spatiotemporal resolution (~350 nm and 2 min/image) for a prolonged duration (>24 hours), we established a live-cell imaging approach based on lattice light-sheet microscopy (Fig 1A, Movie EV1, see also Appendix Fig S1 for comparison with confocal microscopy). This approach produced a live-cell movie library of the non-transformed human cell line RPE-1 under four different conditions: 1) "CENP-E reactivated", obtained by reactivating CENP-E motor activity after its inhibition by the small-molecule inhibitor GSK923295 (Wood *et al*, 2010) and subsequent wash-out, 2) "CENP-E depleted", obtained by depletion of CENP-E by the use of small interfering RNAs (siRNAs), 3) "CENP-E inhibited", obtained by continuous inhibition of CENP-E by GSK923295, and 4) "control", treated just with DMSO (Fig 1B). We then tracked the 3D positions of centrosomes and kinetochores over time in randomly selected cells (see Methods). The depletion effectiveness for all targets throughout the manuscript is provided in Appendix Fig S2A-H.

We reasoned that if chromosome congression is driven by CENP-E, the movement of polar chromosomes would differ in the presence or absence of CENP-E activity. Conversely, if CENP-E is involved in other processes essential for congression but not directly in the movement itself, the movement would be similar regardless of CENP-E activity (Fig 1C). Following reactivation of CENP-E, all polar chromosomes successfully congressed to the metaphase plate during 60 min (Fig 1D, Appendix Fig S1A, Movie EV2). Polar kinetochores approached the equatorial region in a highly uniform manner, characterized by an initial slower and faster second phase of movement (Fig 1D, Appendix Fig S1A) (Kapoor *et al*, 2006), gradual increase in interkinetochore distance (Appendix Fig S1B), and a gradual reorientation of the axis between sister kinetochores toward the main spindle axis (Appendix Fig S1C), similar to kinetochores during early prometaphase in control cells (Fig 1D, Appendix Fig S1A-C, Movie EV2) (Magidson *et al*, 2011), although slower phase of congression was brief or absent in control cells (Fig 1D). We thus conclude that the CENP-E-driven congression of polar chromosomes after CENP-E reactivation recapitulates the main features of their congression during prometaphase.

How do the dynamics of chromosome congression compare between cells with the active and perturbed CENP-E? In CENP-E depleted and CENP-E inhibited conditions, the number of polar chromosomes decayed gradually during mitosis as chromosomes congressed to the metaphase plate (Fig 1D, Movie EV3), resulting in successful congression of majority of polar chromosomes within 3 hours, similar to previous observations (Tovini & McClelland, 2019; Maia *et al*, 2010; Barisic *et al*, 2014; Kim *et al*, 2010). Intriguingly, although asynchronous over

prolonged mitosis (Fig 1D), the movement of polar kinetochores toward the plate was highly similar between conditions with active and perturbed CENP-E (Fig 1D, Appendix Fig S1D, Movie EV3), and was accompanied by an increase in interkinetochore distance and reorientation of the kinetochore pair towards the spindle axis in all conditions (Fig 1D, Appendix Fig S1A-D). Furthermore, the mean velocities of sister kinetochore movement during 6 minutes before joining the plate, which corresponds to the major part of the congressional movement (Fig 1D, Appendix Fig S1A-D), were indistinguishable between conditions (Fig 1E). This implies that polar chromosomes move from the spindle poles to the equator in a manner independent of CENP-E activity, arguing against models where CENP-E actively moves polar chromosomes by gliding them along spindle microtubules.

Since we observed that congression movement remains highly similar regardless of CENP-E activity, our next objective was to understand why the absence of CENP-E leads to extensive delays in chromosome congression. We discovered that less than 20% of polar kinetochores initiated congression in a 30 min period following the end of prometaphase spindle elongation in the CENP-E perturbed conditions. In comparison, more than 70% of polar chromosomes initiated congression when CENP-E was reactivated, and 100% did so under control condition (Fig 1F, Appendix Fig S1A-D, Movies EV2 and EV3). This implies CENP-E plays a role in the initiation of kinetochore movement. Additionally, a slightly stronger effect on the frequency of congression initiation is observed when CENP-E is inhibited rather than depleted (Fig 1F). Finally, we tested whether the dynamics of congression changes with the time spent in mitosis. There was no correlation between the velocity of congression and the time elapsed from the onset of mitosis until the congression event across conditions (Appendix Fig S1E), indicating that the dynamics of chromosome movement during congression are robust to the time spent in mitosis. In conclusion, our findings suggest that while CENP-E does not move polar chromosomes during congression, it is crucial for the rapid and synchronous initiation of this movement.

**CENP-E triggers the transition from lateral to end-on microtubule attachments**

Since we identified that chromosome congression consists of initiation and movement phases, we hypothesized that the initiation phase involves the formation of end-on attachments at polar kinetochores. This led us to propose that CENP-E has an active role in establishing end-on microtubule attachments at polar kinetochores, rather than maintaining lateral attachments, as previously suggested (Shrestha & Draviam, 2013). To explore this hypothesis, we reactivated CENP-E in cells expressing the SAC protein Mad2, which accumulates on kinetochores lacking end-on attachments (Chen *et al*, 1996; Collin *et al*, 2013; Kuhn & Dumont, 2017), to track the response of kinetochore microtubule attachments to CENP-E reactivation over time. Immediately after CENP-E reactivation, polar kinetochores had high levels of Mad2, indicating the absence of end-on attachments (Fig 2A and B, Fig EV1A) (Barisic *et al*, 2014). As a response to CENP-E reactivation, Mad2 levels on polar kinetochores gradually decreased over time (Fig 2A and B, Fig EV1A, Movie EV4), in contrast to the cells in which CENP-E was continuously inhibited and Mad2 levels remained constant (Fig EV1B). Interestingly, the drop of Mad2 on polar kinetochores started, on average, prior to their fast movement towards the equatorial plane (Fig 2B, Fig EV1C-E). In line with that, Mad2 dropped also on kinetochores that did not initiate movement during the

imaging, though at a slower rate (Fig EV1C and D). These results imply that the formation of end-on attachments on polar kinetochores depends on CENP-E activity, and occurs before the congression movement of the kinetochore.

If end-on conversion is coupled to congression than congressing chromosomes would predominantly come to the equatorial plate already bioriented. Indeed, the average Mad2 signal on sister kinetochores after CENP-E reactivation was higher at the kinetochore pairs that were closer to the spindle pole, and the majority of kinetochores approached the metaphase plate with Mad2 signal intensities indistinguishable from those of aligned kinetochores (Fig 2C and D). The Mad2 signal was negatively correlated with the distance between sister kinetochores, which serves as a readout of inter-kinetochore tension (Fig EV1F). These results suggest that after CENP-E is reactivated, polar kinetochores progressively establish more end-on attachments with microtubules, generating increased tension on the kinetochores (Kuhn & Dumont, 2017). If the extent of end-on conversion is dictating dynamics of congression, then the average congression speed over a longer period, which reflects whether or not end-on conversion occurred, is expected to be correlated with Mad2 loss. Indeed, the speed of kinetochore movement during 30 minutes after CENP-E reactivation was correlated with the rate of Mad2 loss (Fig 2E), suggesting that the speed of congression initiation is dictated by the rate of formation of end-on attachments, which is reflected in the rate of Mad2 loss.

Furthermore, we hypothesized that the fibrous corona, a dense protein meshwork forming on kinetochores in the absence of end-on microtubule attachments (Gassmann, 2023; McAinsh & Kops, 2023), might inhibit chromosome congression. To test if the corona inhibits congression in our assays, we compared the mean levels of CENP-E, used as a corona marker (Wu *et al*, 2023; Cmentowski *et al*, 2023) and Mad2 on kinetochores following CENP-E inhibition, CENP-E depletion (note that here Zw10 was used as a corona marker, see below), and in control cells (Fig 2F). Our analysis revealed a strong correlation between Mad2 and CENP-E levels on polar kinetochores in both control and CENP-E-inhibited cells (Fig 2G, Fig EV1G). The average levels of both proteins were significantly higher in CENP-E-inhibited cells (Fig 2G, Fig EV1G). Surprisingly, in CENP-E-depleted cells, the level of Mad2 on polar kinetochores remained similar to that in CENP-E-inhibited cells despite a significant reduction in the amount of kinetochore CENP-E (Fig 2G, Fig EV1G). In line with this, by using the RZZ complex component Zw10 as a marker of the corona (Cmentowski *et al*, 2023; Sacristan *et al*, 2018), we observed excessive recruitment of Zw10 to polar kinetochores compared to control prometaphase cells, especially after depletion of CENP-E (Fig 2H and I, Fig EV1H). These findings suggest that without CENP-E, corona extensively expands on polar kinetochores, contributing to the obstruction of end-on conversion (Cheerambathur *et al*, 2013).

To directly test if congression is coupled with biorientation, we performed super-resolution imaging of spindle microtubules by using Stimulated Emission Depletion (STED) microscopy in CENP-E inhibited cells, and after reactivation of CENP-E at two time-points in RPE-1 and cancer osteosarcoma U2OS cells, to observe and quantify different types of microtubule attachments to kinetochores during chromosome congression (Fig 2J, Fig EV1I). The reactivation of CENP-E was accompanied by chromosome congression and a gradual change from lateral to end-on

attachments on polar chromosomes in RPE-1 (Fig 2J and K), and U2OS cells (Fig EV1I), while the attachment status on aligned kinetochores remained unchanged (Fig EV1L). The interkinetochore distance together with the fraction of bioriented kinetochores progressively increased with the distance from the centrosome until a distance of about 2.5 µm, after which nearly all polar kinetochores were bioriented (Fig 2L). In CENP-E-inhibited cells (Fig 2J, EV1J and K), congressing chromosomes situated between the metaphase plate and the spindle pole, which represented less than 5% of all polar chromosomes, were also bioriented (Fig 2J, Fig EV1J-N). Collectively, our results demonstrate that chromosome movement during congression depends on shifting from lateral to end-on kinetochore-microtubule attachments, with CENP-E playing an important role in accelerating this process (Fig 2M).

**Aurora kinases delay chromosome congression in the absence of CENP-E activity**

Having shown that CENP-E promotes end-on attachments to initiate chromosome congression, we aimed to systematically test the hierarchy of molecular events involved in this process by acute inhibition experiments (Fig 3A). We proposed that a signaling pathway inhibits stabilization of end-on attachments in the absence of CENP-E, thereby preventing congression. Consequently, if end-on conversion is initiated without CENP-E, we expected polar chromosomes to undergo congression. To test this, we inhibited Aurora B kinase that counteracts formation of end-on attachments (Shrestha *et al*, 2017), and maintenance of the Mad1:Mad2 as well as RZZ complex on kinetochores (Maia *et al*, 2010; Shrestha *et al*, 2017; Cheerambathur *et al*, 2013; Famulski & Chan, 2007). Fascinatingly, after acute inhibition of aurora B by 3µM ZM-447439 (Ditchfield *et al*, 2003) in both CENP-E-inhibited and depleted conditions, polar chromosomes immediately started moving and most of them completed congression within 30 minutes after the addition of the inhibitor (Fig 3B-D, Fig EV2A-F, Movie EV5). A small fraction of polar chromosomes did not reach the metaphase plate but ended their journey close to the plate (Fig 3B, Fig EV2F), probably due to deficient correction of attachment errors (Lampson *et al*, 2004). These results imply that polar chromosomes initiate congression instantly without CENP-E if end-on conversion is allowed by the acute inhibition of Aurora B.

Chromosome congression after acute inhibition of Aurora B in the absence of CENP-E activity was neither dependent on the premature onset of anaphase that was blocked by the usage of proteasome inhibitor MG132 (Santaguida *et al*, 2011) (Fig EV2G), nor the lower concentration (Fig EV2H) and specificity of Aurora B inhibitor (Yang *et al*, 2007) (Fig EV2I). Furthermore, the depletion of the cohesion release factor WAPL (Hengeveld *et al*, 2017) (Fig EV2J), the co-depletion of the chromokinesins Kid/kinesin-10 and Kif4a/kinesin-4 (Barisic *et al*, 2014) (Fig 3C, Fig EV2K), nor the acute inhibition of Protein phosphatases 1 and 2A (PP1/PP2A) by Okadaic acid (Su *et al*, 2016) (Fig 3C, Fig EV2K and L) did not stop chromosomes from initiating and finishing congression after acute inhibition of Aurora B. This implies that the loss of centromeric cohesion (Hindriksen *et al*, 2017), the polar ejection forces generated by chromokinesins on chromosome arms (Drpic *et al*, 2015; Cane *et al*, 2013) and the activity of phosphatases (Ehlén *et al*, 2020) are not essential for congression movement after acute inhibition of Aurora B.

Interestingly, chromosome congression in the absence of both CENP-E and Aurora B activity was marked by rapid movement of polar kinetochores toward the equatorial plane, that

was indistinguishable in velocity from other CENP-E perturbations (Fig 3D, Fig EV2A-B and M). However, a distinctive feature of congression without Aurora B activity was the absence of the slower initial phase of congression (Fig EV2A and B). This indicates that only the initiation of congression after CENP-E reactivation requires Aurora B activity, suggesting that CENP-E initiates chromosome congression by down-regulating Aurora B activity.

To gain further insight into signaling that limits chromosome congression in the absence of CENP-E, we co-inhibited or depleted various molecular regulators that are involved in the regulation of biorientation or Aurora B recruitment (Ali & Stukenberg, 2023) under CENP-E inhibited condition. Interestingly, inhibition of Aurora A kinase, which shares specificity and certain kinetochore targets with Aurora B, most notably the kinetochore protein Hec1 (Highly expressed in cancer 1) (Ye *et al*, 2015) induced congression of polar chromosomes in the absence of CENP-E, although much slower than acute Aurora B inhibition (Fig 3B-D, Movie EV5). On the other hand, inhibition and co-inhibition of Bub1 (Budding uninhibited by benzimidazoles 1) or Haspin, factors essential for the recruitment of Aurora B to the outer and inner centromere, respectively (Dai *et al*, 2005; Kawashima *et al*, 2007; Broad *et al*, 2020; Hadders *et al*, 2020), did not induce chromosome congression in the absence of CENP-E activity, as well as inhibition of Polo-like kinase 1 (Plk1) kinase, and depletion of Bub1-related (BubR1) pseudokinase (Fig 3C, Fig EV2N). The only other kinase whose inhibition showed a minor but statistically nonsignificant effect compared to the control group was Monopolar spindle 1 (Mps1) kinase (Fig 3C, Fig EV2N). This implies that centrosome localized Aurora A and the outer-kinetochore localized Aurora B are major factors that limit the initiation of congression in the absence of CENP-E.

Perturbations of microtubule motor proteins, including dynein (Barisic *et al*, 2010; Gassmann *et al*, 2010; Firestone *et al*, 2012), Kid, Kif4a, Eg5 and the crosslinker of antiparallel microtubules PRC1 (Kajtez *et al*, 2016; Polak *et al*, 2017) revealed that neither their indirect nor direct perturbations induced congression of polar chromosomes in the absence of CENP-E (Fig 3C, Fig EV2N and O). These results suggest, respectively, that the poleward pulling forces exerted by kinetochore dynein, the activity of chromokinesins, the distance between the plus ends of microtubules nucleated in one spindle half and the opposite spindle pole, and the thickness of antiparallel microtubule bundles to which kinetochores are initially laterally attached (Matković *et al*, 2022), are not major obstacles to congression in the absence of CENP-E activity. Instead, the primary barrier to congression without CENP-E is the activity of Aurora kinases.

To test if BuBR1, a known interactor of PP2A and CENP-E (Shrestha *et al*, 2017; Suijkerbuijk *et al*, 2012; Kruse *et al*, 2013; Legal *et al*, 2020), is required for congression initiation after Aurora B inhibition, we acutely inhibited Aurora B in the absence of CENP-E and BubR1. Interestingly, congression of polar chromosomes was completely stopped after Aurora B inhibition in BuBR1-depleted and CENP-E-inhibited cells, contrary to cells where BuBR1 was intact (Fig 3C). These results suggest that BuBR1 is crucial for initiation of chromosome congression independently of CENP-E recruitment (Legal *et al*, 2020), and that its absence cannot be overturned by the inhibition of Aurora kinases. This indicates that the interaction of BubR1 with PP2A might be crucial for initiation of congression. However, we did not find evidence implicating protein phosphatases play a role in this process by direct phosphatase inhibition experiments.

Finally, we directly tested the possible role of corona expansion in inhibiting congression initiation by quantifying Zw10 on polar kinetochores after CENP-E perturbations and acute inhibition of Aurora B kinase. We found that acute Aurora B inhibition led to a strong drop of Zw10 on polar kinetochores, both after CENP-E inhibition and depletion (Fig 2I, Fig EV1H). These results corroborate our conclusion that the excessive expansion of the kinetochore corona in the absence of CENP-E or its activity contributes to the inhibition of chromosome congression initiation, which can be relieved by Aurora B inhibition.

**CENP-E initiates chromosome congression in a manner dependent on Hec1 and BubR1**

We next used the CENP-E reactivated condition to test which molecular factors regulate chromosome congression upstream and downstream of CENP-E in a time-dependent manner (Fig 3E). As a first hypothesis, we assumed that the role of CENP-E in the initiation of chromosome congression reflects the recruitment of protein phosphatases to the outer kinetochore, either directly or through its interaction with BubR1 (Kim *et al*, 2010; Song *et al*, 2021). However, acute or 30-minute long inhibition (see Methods) of PP1/PP2A activities by Okadaic acid did not prevent chromosome congression after reactivation of CENP-E (Fig 3F and G, Fig EV3A and B, Movie EV5), similarly to the finding that inhibition of PP1 in HeLa cells during prometaphase did not block congression of polar chromosomes (Kim *et al*, 2010). Congression after CENP-E reactivation was also successful without the activities of Plk1 kinase which regulates microtubule dynamics (Salimian *et al*, 2011), Kif18a/kinesin-8, which promotes chromosome alignment at the metaphase plate (Stumpff *et al*, 2008), or the chromokinesins Kid and Kif4a and thus the polar ejection forces they generate (Drpic *et al*, 2015) (Fig 3G, Fig EV3C).

Phosphorylation of CENP-E mediated by Aurora kinases was previously reported to be crucial for the motor activity of CENP-E during congression (Kim *et al*, 2010). However, polar chromosomes were able to congress after reactivation of CENP-E when Aurora B kinase was acutely inhibited (Fig 3G, Fig EV3C and D). Similar to the acute inhibition of Aurora B in the absence of CENP-E activity (Fig 3B-D), congression after acute inhibition of Aurora B in the presence of CENP-E activity was occasionally characterized by an incomplete congression of polar chromosomes (Fig EV3C and D), suggesting that problems in error correction that are the result of Aurora B inhibition (Lampson *et al*, 2004) limit complete congression of some polar chromosomes. To sum up, polar chromosomes can initiate congression when total Aurora B is inhibited, irrespective of CENP-E activity.

It is unknown whether CENP-E activity requires the presence of lateral attachments to mediate congression, as would be expected if CENP-E acts through the establishment of end-on attachments. To increase the number of polar chromosomes with prematurely stabilized end-on attachments, we reactivated CENP-E in cells depleted of Spindly, a kinetochore adaptor of dynein (Gassmann *et al*, 2010; Barisic *et al*, 2014) that is also involved in the recruitment of CENP-E on kinetochores (Cmentowski *et al*, 2023). The proportion of polar chromosomes that congressed after CENP-E reactivation was significantly lower in Spindly-depleted cells compared to controls (Fig 3G, Fig EV3E). This indicates that CENP-E cannot initiate the congression of polar kinetochores with stable end-on attachments or that Spindly recruits CENP-E on kinetochores (Cmentowski *et al*, 2023).

To challenge our model in which congression requires biorientation, we asked whether CENP-E facilitates chromosome movement independently of end-on attachments in cells depleted of Hec1 and KifC1/HSET, a condition reported to allow chromosome pseudoalignment without end-on attachments (Cai *et al*, 2009). We then combined this approach with perturbations of CENP-E, followed by an analysis of chromosome alignment and Hec1 kinetochore levels in individual mitotic cells using immunofluorescence. Our results show that chromosome alignment improved after depletion of HSET in Hec1-depleted cells, whereas additional CENP-E depletion caused severe misalignment (Fig 3H and I, Fig EV3F-H), similar to the previous report (Cai *et al*, 2009). However, we observed that the degree of chromosome alignment strongly correlated with the level of residual Hec1 at the kinetochores (Fig 3J), which was typically higher in Hec1- and HSET-codepleted cells than after Hec1 depletion alone (Fig EV3G and H). Importantly, cells with minimal Hec1 on kinetochores exhibited large misalignments regardless of HSET or CENP-E codepletions (Fig 3H and J). In agreement, the movement of polar chromosomes in Hec1-depleted cells did not depend on CENP-E activity as the chromosomes moved in a similar manner in Hec1-depleted cells and Hec1-depleted and CENP-E-inhibited cells (Fig 3K), similar to a previous report in HeLa cells (Iemura & Tanaka, 2015). This indicates that a small level of Hec1 on a kinetochore, 10-15% of control level, is sufficient to promote congression and that the function of CENP-E in chromosome congression is dependent on the presence of Hec1.

Lastly, we tested the requirement for BubR1 during CENP-E-mediated congression of polar chromosomes. We depleted BubR1 and inhibited CENP-E together with MG132 treatment to prevent the premature onset of anaphase (Lampson & Kapoor, 2005). Reactivation of CENP-E activity in BubR1-depleted cells did not result in congression of polar chromosomes (Fig 3F and G, Fig EV3B, Movie EV5). This finding, together with our observation that BubR1 is required to counteract Aurora B independently of CENP-E recruitment (Fig 3C), suggests that BubR1 is crucial for the lateral-to-end-on conversion and subsequent chromosome congression - likely due to its role in recruiting PP2A, which counteracts Aurora kinase activity (Kruse *et al*, 2013). However, we did not observe the effect on congression with direct phosphatase inhibition.

**Centrioles inhibit chromosome congression in the absence of CENP-E**

As polar chromosomes in the absence of CENP-E remain localized close to centrosomes for a prolonged duration (Barisic *et al*, 2014) and since their chance to initiate congression is positively correlated with the distance from the centrosome (Appendix Fig S1F and G), we hypothesized that centrosomes inhibit congression of polar chromosomes in the absence of CENP-E activity. We thus reasoned that the depletion of centrioles, focal constituents of centrosomes (Vasquez-Limeta & Loncarek, 2021), could release polar chromosome congression from its dependence on CENP-E. To deplete centrioles, we inhibited polo-like kinase 4 (Plk4) activity with centrinone, a small molecule inhibitor that blocks the centriole duplication cycle (Wong *et al*, 2015), and varied the duration of treatment to obtain spindle types with different numbers of centrioles on each pole, namely 2:2, 1:1, 1:0 and 0:0 (Fig EV4A), and combined it with CENP-E perturbations.

As a proxy of congression efficiency, we quantified the number of polar chromosomes 5 minutes after the end of spindle elongation, the residence time of polar chromosomes on spindle poles, and the total duration of mitosis. After CENP-E perturbations, 1:1 and 2:2 spindles had, on

average, about 8 polar chromosomes per spindle, whereas this number was <1 in control conditions in both spindle types (Fig 4A and B, Movie EV6). In 1:0 spindles, the centriolar poles (labeled "1") contained approximately 4 polar chromosomes, similar to the equivalent poles in 1:1 spindles (Fig 4B, Movie EV6). In contrast, the acentriolar poles (labeled "0") in 1:0 spindles had, on average, ~1 polar chromosome, regardless of CENP-E activity (Fig 4A and B, Movie EV6). Polar chromosomes persisted much longer on centriolar then on acentriolar poles across all spindle types when CENP-E was perturbed (Fig 4C), causing extensive mitotic prolongation (Fig EV4B). Completely acentriolar 0:0 spindles, which were rarely found due to p53-dependent arrest (Wong *et al*, 2015), had a low number of polar chromosomes in the CENP-E inhibited condition, indistinguishable from acentriolar poles in 1:0 spindles (Fig 4D and E, Movie EV6). These findings suggest that centrioles specifically limit the congression of polar chromosomes if CENP-E activity is perturbed.

The inhibitory effect of centrioles on polar chromosome congression without CENP-E in 1:0 spindles was independent of passage through the transient monopolar state (Dudka *et al*, 2019), as indicated by the unchanged number of CENP-E-dependent polar chromosomes after forced transient monopolarization via Eg5 inhibitor washout and inhibition of CENP-E (Fig 1D and Fig EV4C). Furthermore, we did not observe a difference in microtubule organization on centriolar and acentriolar poles when imaging microtubules by STED microscopy, except a lack of centrioles and astral microtubules on the acentriolar pole (Fig EV4D). We also compared the dynamics of congression in 1:0 and 1:1 spindles in the CENP-E inhibited condition, and found that congression velocities were indistinguishable from each other, and from the velocity after CENP-E inhibition in 2:2 spindles (Fig EV4E-J). This suggests that the velocity of chromosome congression is robust to changes in the number of centrioles.

We investigated whether centriole dislocation during prolonged mitosis induces congression of polar chromosomes independently of long-term Plk4 inhibition effects. To do this, we focused on rare cases (<10%, n=5 out of 55 cells) where spontaneous acute dislocation of a centriole from the centrosome in 1:1 spindles occurred in the CENP-E depleted condition (Fig EV4K) (McEwen *et al*, 2001). Fascinatingly, upon displacement of a centriole from the centrosome, polar chromosomes initiated congression almost instantaneously in all cases (Fig EV4K). This suggests that the presence of centrioles *per se* limits the congression of polar chromosomes in the absence of CENP-E. To conclude, the presence of centrioles is required for persistence of polar chromosomes in the absence of CENP-E activity (Fig 4F), demonstrating that centrioles inhibit the congression of polar chromosomes.

**Centriolar Aurora A increases kinetochore Aurora B activity, leading to increased KMN network phosphorylation and delayed congression initiation in the absence of CENP-E**

To identify molecular factors that delay chromosome congression on centriolar poles in the absence of CENP-E, we checked the levels of active Aurora A on spindle poles after Plk4 inhibition under both control and CENP-E inhibited conditions. Intriguingly, we found that acentriolar poles had a 4-fold lower levels of pAurA (pT288-Aurora A) compared to centriolar poles, whereas the maximum difference between two poles in 1:1 spindle was on average only 10% (Fig 5A). The observed difference in pAurA between poles was not CENP-E dependent (Fig

5A and Fig EV5A), implying that CENP-E does not control the level of active Aurora A on spindle poles. These results, together with our observation that Aurora A inhibition induces congression in the absence of CENP-E (Fig 3C), demonstrate that polar chromosomes depend on CENP-E activity for congression due to a high activity of Aurora A close to centrosomes.

We hypothesized that the difference in Aurora A activity between centriolar and acentriolar spindle poles causes varying activation of kinetochore-localized Aurora B kinase on polar chromosomes. This activation subsequently affects the phosphorylation of Aurora B downstream targets, Hec1 and Knl1, which are major components of the KMN network (Navarro & Cheeseman, 2021). Indeed, the mean signal of pAurB (pT232-Aurora B) and pKnl1 (pS24, pS60-Knl1) (Welburn *et al*, 2010) on polar kinetochores close to centriolar poles was significantly higher compared to the signal on aligned kinetochores and on rare polar kinetochores at the acentriolar poles under the CENP-E inhibited condition (Fig 5B-D, Fig EV5B-E). For pHec1 (pS55-Hec1) (DeLuca *et al*, 2006) a significant difference was observed only between polar and aligned kinetochores (Ye *et al*, 2015) (Fig 5B-D, Fig EV5B-E). In control cells, the level of phosphorylation was similar between aligned and rare polar kinetochores for pAurB, pKnl1 and pHec1, and was significantly lower compared to the same kinetochore groups in the CENP-E inhibited condition for pAurB and pKnl1 (Fig 5B-D, Figure EV5B-F). Our results imply that in the absence of CENP-E activity, Aurora A on centriolar poles increases the activity of outer-kinetochore Aurora B. This, in turn, increases the phosphorylation of downstream outer-kinetochore proteins like Knl1, and to a lesser extent Hec1, which limits the end-on binding of microtubules to the kinetochores and subsequently their congression.

We also directly examined whether Aurora A regulates the activity of Aurora B on polar kinetochores in the absence of CENP-E activity, by inhibiting Aurora A in CENP-E-inhibited cells, staining the pAurB by immunofluorescence, and quantifying its levels on kinetochores at various time points (Fig 5E). The results showed that inhibiting Aurora A markedly decreased Aurora B activity on polar kinetochores, bringing it down to levels observed on aligned kinetochores in the absence of CENP-E activity (Fig 5E and F, Fig EV5G). These results support the model in which, without CENP-E, Aurora A activates Aurora B near the spindle poles. The high activity of Aurora B leads to the inhibition of end-on attachments and subsequent mitotic delays.

To test if Aurora kinases inhibit congression directly through the regulation of Hec1 phosphorylation status, we used HeLa cells engineered to express an inducible, siRNA-resistant GFP-Hec1-9A mutant (Etemad *et al*, 2015) that mimics constitutive dephosphorylation (DeLuca *et al*, 2011). Given our previous findings, we predicted that constitutive dephosphorylation of Hec1 might compensate for disruptions in CENP-E function. Indeed, we observed that expressing non-phosphorylatable Hec1-9A in a background of endogenous Hec1 depletion (Fig EV5H) improved chromosome alignment following CENP-E depletion, though not after CENP-E inhibition (Fig 5G and H). This suggests that phosphorylation of Hec1 by Aurora kinases specifically hinders congression in the absence of CENP-E, aligning with our previous results using acute kinase inhibition.

If Aurora A at the centrosomes increases the activity of Aurora B, then the movement of chromosomes away from the centrosome during congression should be accompanied by a gradual

decrease in Aurora B-mediated phosphorylation of outer kinetochore targets. Indeed, the level of Aurora B-mediated phosphorylation of the pKnl1 was inversely correlated with the distance of the chromosome from the centrosome in the absence of CENP-E activity (Fig EV5I). To conclude, we show that chromosome congression is accompanied by a decrease in Aurora B activity on kinetochores resulting in a decreased phosphorylation of the KMN network components, a process essential for stable attachment of microtubules to kinetochores (Fig 5I) (Cheeseman *et al*, 2006) and chromosome congression, which is drastically accelerated by the CENP-E motor activity.

**Mitotic duration defines high sensitivity to CENP-E perturbations in cancer cells**

Our results thus far demonstrate that congression of polar chromosomes in healthy cells is initiated by a lateral to end-on conversion, where CENP-E accelerates the essential first steps of this process. This leads to a gradual reduction of phosphorylation of the outer kinetochore proteins mediated by Aurora B kinase and subsequently chromosome biorientation. However, it remains unknown whether the described congression dynamics would hold true in cancer cell lines, which are often characterized by perturbed microtubule dynamics and deficient error correction (Bakhoum *et al*, 2009; Salimian *et al*, 2011; Ertych *et al*, 2014). To explore the response of transformed cell lines to varying levels of CENP-E activity, we examined the movement of polar chromosomes following CENP-E reactivation, CENP-E perturbations and in the control U2OS tumor cells (Fig 6A, Appendix Fig S3A and B).

First, we observed that U2OS cells displayed polar chromosomes that congressed asynchronously after CENP-E depletion causing extensive mitotic prolongations (Fig 6A, Movie EV7), similar to RPE-1 (Fig 1A), and previous reports in HeLa cells (Maia *et al*, 2010; Gomes *et al*, 2022). Interestingly, and consistently with RPE-1, movement of chromosomes during congression in all parameters was similar across all conditions independently of CENP-E activity (Fig 6B and C, Appendix Fig S3C-E). Likewise, the velocity of congression 4 minutes before the polar chromosome entered the plate was indistinguishable between conditions with perturbed and active CENP-E (Fig 6D), similar to RPE-1 (Fig 1E). However, the mean congression velocities were ∼1.8 times faster in U2OS (Fig 6D) than the mean velocities in the same conditions in RPE-1 (Fig 1E). Similar to RPE-1 (Appendix Fig 1E), congression velocities did not depend on the time elapsed from the onset of mitosis until the congression event in the CENP-E depleted condition (Appendix Fig S3F). From these results, we concluded that the congression movement in U2OS cells is also CENP-E independent but is significantly faster than in RPE-1 cells.

Next, we examined how efficiently U2OS cells initiate congression of polar chromosomes compared to RPE-1 cells in the absence of CENP-E. We found that U2OS and RPE-1 cells exhibit a similar gradual decay of the number of polar chromosomes up until ∼1 hour from the onset of mitosis (Fig 6E, Appendix Fig S3G). Both cell lines had a high number of polar chromosomes 20 minutes after the onset of mitosis in the absence of CENP-E (9.86±4.72 in RPE-1, versus 7.72±4.92 in U2OS, Appendix Fig S3H), demonstrating their sensitivity to the absence of CENP-E during early mitosis. However, ∼1 hour after mitotic onset, U2OS cells abruptly lost the ability to initiate congression of polar chromosomes in the absence of CENP-E, since congression events were rarely observed after this point (Fig 6E, Appendix Fig S3G, Movie EV7), while congression in RPE-1 cells continued for hours with almost unchanged dynamics (Fig 6E). This suggests that

U2OS cells have a critical time window for chromosome congression that is highly dependent on CENP-E, whereas RPE-1 cells can sustain congression for longer times even in the absence of CENP-E, indicating a mitotic timing mechanism that differs between these cell lines.

Finally, we asked whether the large difference between the cell lines in congression initiation during prolonged mitosis in the absence of CENP-E induces distinct mitotic outcomes. Indeed, we found that U2OS cells entered anaphase with uncongressed polar chromosomes more often than RPE-1 cells (42% versus 18%, respectively, Fig 6F), similar to previous reports on U2OS and HeLa cells (Maia *et al*, 2010; Gomes *et al*, 2022). We also observed that the severity of mitotic outcomes was time-dependent (Appendix Fig S3I). After similar mitotic delays (Appendix Fig S3I), U2OS cells entered anaphase with ~13 times more polar chromosomes than RPE1 cells upon CENP-E depletion (1.56±2.61 for U2OS versus 0.12±0.32 for RPE-1, Fig 6G). We conclude that the high sensitivity of U2OS cells to the absence of CENP-E drastically reduces mitotic fidelity in this cancer cell line.

## DISCUSSION

For nearly two decades, the model proposing that chromosomes are transported towards the spindle equator without biorientation by kinetochore molecular motors like CENP-E has stood the test of time and remained unchallenged (Kapoor *et al*, 2006), inspiring many exciting models of chromosome movement and its regulation (Barisic *et al*, 2014, 2015; Cai *et al*, 2009; Kim *et al*, 2010; Eibes *et al*, 2023; Gudimchuk *et al*, 2013). Here, we present systematic evidence supporting an alternative model where chromosome movement depends on biorientation (Fig 7), aligning with pioneering propositions on the topic (McEwen *et al*, 2001, 1997). In this model, CENP-E enhances the formation or stabilization of end-on attachments on polar chromosomes, thereby promoting rapid biorientation and synchronous chromosome congression during early mitosis (Fig. 7). These conclusions are based on the following results: 1) chromosome congression movement has the same dynamics regardless of CENP-E presence or activity; 2) end-on attachments form and the Mad2 signal drops on polar kinetochores prior to their movement; 3) all congressing chromosomes are bioriented a few microns from the centrosome, as visualized by STED microscopy; 4) CENP-E has limited ability to drive chromosome movement without end-on attachments or if they are prematurely stabilized; 5) congression initiates without CENP-E if Aurora kinases are inhibited, which forces biorientation; 6) BubR1 is essential for chromosome congression regardless of CENP-E recruitment, likely due to its role in recruiting phosphatases and opposing Aurora B kinases; and 7) the requirement for CENP-E during congression can be bypassed by removing centrioles, thus lowering Aurora A activity, or by increasing the fraction of constitutively dephosphorylated Hec1, thus bypassing Aurora B activity.

The presented model of chromosome congression movement is based on two interconnected molecular feedback loops involving centrosome and kinetochore components (Fig 7). First, Aurora A activity near centrioles upregulates Aurora B activity on the outer kinetochore, likely via phosphorylation. Activated Aurora B limits end-on attachment stability by phosphorylating KMN network components (DeLuca *et al*, 2011; Shrestha *et al*, 2017) and regulating the RZZ complex and fibrous corona expansion (Famulski & Chan, 2007; Cheerambathur *et al*, 2013). Aurora A also directly phosphorylates KMN near centrioles (Ye *et al*, 2015). This signaling axis, combined with back-to-back kinetochore organization (Lončarek *et al*, 2007), prevents premature erroneous end-on attachments near centrosomes (Ye *et al*, 2015; Barisic *et al*, 2014) that would impede congression. Second, Aurora kinases phosphorylate and activate CENP-E near centrioles (Kim *et al*, 2010; Eibes *et al*, 2023). We speculate that the activated CENP-E interacts with BubR1-PP2A (Huang *et al*, 2019), and activity of PP2A leads to downregulation of Aurora B kinase activity, and net dephosphorylation of its substrates, primarily Knl1 and to a lesser extent Hec1. This stabilizes early end-on attachments on polar kinetochores, indicated by the start of Mad2 loss, and initiates congression movement. Recently, it was shown that CENP-E has distinct pools on kinetochore and fibrous corona (Cmentowski *et al*, 2023), recruited by BubR1 and RZZ complex, respectively (Legal *et al*, 2020; Cmentowski *et al*, 2023; Weber *et al*, 2024). Since congression initiation depends on BubR1, we suggest it is primarily driven by the kinetochore-localized CENP-E.

We propose that in addition to phosphorylating KMN network components, Aurora kinases inhibit the stabilization of end-on attachments by promoting the expansion of the fibrous corona on unattached chromosomes (Fig 7). Previously, it was proposed that competition between corona components and Ndc80 regulates microtubule engagement and end-on conversion (Cheerambathur *et al*, 2013). Recent studies indicate that CENP-E is crucial for expanding the fibrous corona (Wu *et al*, 2023; Cmentowski *et al*, 2023) which can nucleate and sort microtubules (Renda *et al*, 2022; Wu *et al*, 2023) or serve as a hub for capturing microtubules (Sacristan *et al*, 2018). However, our results, obtained in the presence of formed spindles, unlike previous studies with depolymerized microtubules, demonstrate that the corona expands without CENP-E or its activity. Instead, we suggest that extensive corona expansion inhibits end-on attachments and chromosome congression in the absence of CENP-E, supported by our and previous observations that excessive corona is almost completely removed upon acute Aurora B inhibition (Famulski & Chan, 2007). However, our results show that Spindly removal in CENP-E perturbed cells is insufficient to initiate congression. Similarly, inhibiting Mps1, a key regulator of corona assembly (Sacristan *et al*, 2018), has a less pronounced effect on congression initiation compared to inhibiting Aurora kinases. These results suggest that the expansion of the fibrous corona has a secondary effect in preventing end-on attachments compared to the phosphorylation of the KMN network.

Our model predicts that chromosome congression can initiate without CENP-E activity if the KMN network has maximum microtubule affinity, and the fibrous corona disassembles (Fig 7). We have shown that this occurs after Aurora kinase inhibition for polar chromosomes, but it is also observed in untreated cells during early mitosis for chromosomes that are located far from the spindle pole (Barisic *et al*, 2014). Those chromosomes are positioned outside the Aurora A gradient, and therefore have lower activity of Aurora B on kinetochores, which can explain their CENP-E-independent congression. Our model does not exclude the possibility that CENP-E can facilitate chromosome movement by gliding polar kinetochores, if they are very close to the pole, along highly detyrosinated microtubules away from the Aurora A gradient (Barisic *et al*, 2014, 2015). However, chromosomes rarely encounter a high Aurora A gradient during unperturbed mitosis in healthy cells (Renda *et al*, 2022), in contrast to cancer cells where some chromosomes are found near centrosomes early in mitosis, resulting in congression delays (Klaasen *et al*, 2022). The fact that chromosomes avoid the region close to the centrosome in healthy cells likely enables rapid chromosome biorientation and congression in those cells.

The coupling between mechanisms governing chromosome congression and chromosome biorientation has remained unclear to date. Previous models of chromosome movement suggested that kinetochore biorientation and chromosome congression are uncoupled processes (Barisic *et al*, 2014; Kapoor *et al*, 2006; Maiato *et al*, 2017). Here, we propose a model where chromosome congression is coupled to biorientation through CENP-E (Fig 7). The notion that CENP-E is involved in end-on conversion has been proposed earlier, in particular that CENP-E maintains lateral attachments (Shrestha & Draviam, 2013). However, our findings demonstrate that CENP-E directly promotes end-on conversion. This model explains why peripheral polar chromosomes experience congression delays without CENP-E (Barisic *et al*, 2014), yet move towards the spindle equator with similar efficiency with and without CENP-E during early mitosis (Renda *et al*, 2022).

The model also aligns with observations that constitutively dephosphorylated Hec1 does not interfere with congression, as the KMN network has maximum microtubule affinity under this condition (DeLuca *et al*, 2011), akin to inhibition of Aurora kinases, and that congression resolves lateral attachments in bipolar spindles induced by forced localization of Aurora B on the outer kinetochore (Shrestha *et al*, 2017). The proposed model provides a molecular mechanism for the spatial and temporal coordination between biorientation and congression. This involves coupling of Aurora kinases, CENP-E, and BubR1 as major drivers or regulators of both processes (Lampson & Kapoor, 2005; Barisic *et al*, 2014; Shrestha *et al*, 2017; Huang *et al*, 2019; Kim *et al*, 2010).

Some important questions regarding chromosome movement during congression remained unanswered. First, if chromosomes move after establishment of biorientation by the forces generated by end-on attached microtubules, what determines the directionality of their movement towards the equator? This bias may be achieved by the microtubule length-dependent activity of Kif18a/kinesin-8 (Stumpff *et al*, 2008) and the length-dependent poleward flux of kinetochore fibers (Risteski *et al*, 2022). Second, what is the exact role of protein phosphatases during congression? We speculate that the CENP-E-mediated down-regulation of Aurora B on kinetochores is independent of tension (Taveras *et al*, 2019), but likely relies on the interaction of activated CENP-E with the BubR1-PP2A complex (Shrestha *et al*, 2017; Huang *et al*, 2019), which competes with Aurora B for substrates on kinetochores. However, our acute phosphatase inhibition experiments did not conclusively demonstrate the essential role of PP2A in congression. Utilizing separation-of-function mutants of CENP-E could resolve this issue.

In the context of mitosis under disease conditions, we discovered that cancer cells exhibit heightened sensitivity to CENP-E inhibitors (Gomes *et al*, 2022) due to their inability to align polar chromosomes after a particular time point during prolonged mitosis. This phenomenon significantly diminishes the mitotic fidelity of these cells, suggesting the presence of distinct mitotic timing mechanisms that impact cancer and non-cancer cells differently. We propose that the duration of mitosis influences the stability of kinetochore microtubules (Bakhoum *et al*, 2009; Kabeche & Compton, 2013) in a manner that impedes congression initiation specifically in CENP-E-deficient cancer cells compared to non-transformed cells during prolonged mitosis. Recent studies have shown that tetraploid cells are more vulnerable to CENP-E inhibitors (Yoshizawa *et al*, 2023) and Kif18a inhibitors (Quinton *et al*, 2021) than diploid cells, likely due to their prolonged mitotic duration (Gliech *et al*, 2024). We hypothesize that these differential effects of kinesin inhibitors stem from distinct responses to mitotic prolongation between chromosomally stable and unstable cells.

## ACKNOWLEDGEMENTS

We thank Alexey Khodjakov, Helder Maiato, Geert Kops, and Jonathon Pines for cell lines; Marin Barišić for intensive discussions and cell lines; Julie Welburn for discussions and antibodies; Magda Topić and Mia Crnogaj for help with cell culture work and preparation of inhibitors; Ivana Šarić for the drawings; and members of the Tolić group and Nenad Pavin group for constructive comments on the manuscript. This work was funded by the European Research Council (ERC Synergy Grant, GA Number 855158), the Croatian Science Foundation (HRZZ) through Swiss-Croatian Bilateral Projects (project IPCH-2022-10-9344), and projects co-financed by the Croatian Government and the European Union through the European Regional Development Fund—the Competitiveness and Cohesion Operational Programme: IPSted (Grant KK.01.1.1.04.0057) and QuantiXLie Center of Excellence (Grant KK.01.1.1.01.0004).

## AUTHOR CONTRIBUTIONS

K.V. and I.M.T conceived the project, K.V. performed all experiments, quantified, analyzed and presented the data, K.V. conceptualized and prepared original draft, K.V. and I.M.T. reviewed, edited and discussed the manuscript.

## METHODS

*Cell lines and culture*

Experiments were carried out using human hTERT-RPE1 (hTERT-immortalized retinal pigment epithelium) cells stably expressing CENP-A-GFP, human hTERT-RPE1 cells stably expressing both CENP-A-GFP and centrin1-GFP and human hTERT-RPE1 cells stably expressing CENP-A-GFP and Mis12-mCherry, all courtesy of Alexey Khodjakov (Wadsworth Center, New York State Department of Health, Albany, NY, USA), human hTERT-RPE1 cells stably expressing CENP-A-mCerulean and Mad2-mRuby, courtesy of Jonathon Pines (Institute of Cancer Research, London, UK), human U2OS (osteosarcoma patient) cells stably expressing CENP-A-GFP, courtesy of Marin Barišić (Danish Cancer Society Research Center, Copenhagen, Denmark), and human HeLa (cervical carcinoma patient) cells expressing GFP-Hec1-9A, courtesy of Geert Kops (Hubrecht Institute, Utrecht, The Netherlands) . All cell lines were cultured in flasks in Dulbecco's Modified Eagle's Medium with 1 g/L D-glucose, pyruvate and L-glutamine (DMEM, Lonza, Basel, Switzerland), supplemented with 10% (vol/vol) heat-inactivated Fetal Bovine Serum (FBS, Sigma-Aldrich, St. Louis, MO, USA) and penicillin (100 IU/mL)/streptomycin (100 mg/mL) solution (Lonza, Basel, Switzerland). The cells were kept at 37 °C and 5% CO2 in a humidified incubator (Galaxy 170 S CO2, Eppendorf, Hamburg, Germany) and regularly passaged at the confluence of 70-80%. None of the cell lines were authenticated. All cell lines have also been tested for mycoplasma contamination once a month by examining samples for extracellular DNA staining with SiR-DNA (100 nM, Spirochrome, Stein am Rhein, Switzerland) and Hoechst 33342 dye (1 drop/2 ml of NucBlue Live ReadyProbes Reagent, Thermo Fisher Scientific, Waltham, MA, USA) and have been confirmed to be mycoplasma free.

*Sample preparation and siRNAs*

At 80% confluence, the DMEM medium was removed from the flask and the cells were washed with 5 ml of phosphate buffered saline (PBS). Then, 1 ml 1% trypsin/ethylenediaminetetraacetic acid (EDTA, Biochrom AG, Berlin, Germany) was added to the flask and cells were incubated at 37 °C and 5% $CO_2$ in a humidified incubator for 5 min. After incubation, trypsin was blocked by adding 4 ml of DMEM medium. For the RNAi experiments, cells were seeded to reach 60% confluence the next day and cultured on 35 mm uncoated plates with 0.17 mm (#1.5 coverglass) glass thickness of 0.17 mm (# 1.5 coverglass) (MatTek Corporation, Ashland, MA, USA) in 1 ml of DMEM medium with the supplements described above. After one day of growth, cells were transfected with either targeting or non-targeting siRNA constructs which were diluted in OPTI-MEM medium (Life Technologies, Waltham, MA, USA) to a final concentration of 100 nM in the medium with cells. All transfections were performed 48 h before imaging using Lipofectamine RNAiMAX Reagent (Life Technologies, Waltham, MA, USA) according to the instructions provided by the manufacturer, unless otherwise indicated. Codepletions of Hec1 or Nuf2 and HSET and CENP-E in RPE-1 cells were performed for two times in two subsequent days by the same protocol. Codepletions of Hec1 and CENP-E in HeLa cells were performed for two times in two subsequent days by the same protocol. After four hours of siRNA treatment, the medium was changed to the prewarmed DMEM medium. GFP-Hec1-9A construct in HeLa cells was expressed by addition of 1 $\mu g\,ml^{-1}$ doxycycline for 24 h prior to fixation. Proteasome inhibitor MG-132

(MedChemExpress, IC50 value 100 nM) at a final concentration of 1 μM, was added 5 h before fixation for experiments involving HeLa GFP-Hec1-9A cells.

The siRNA constructs used were: human CENP-E ON-TARGETplus SMART pool siRNA (L-003252-00-0010, Dharmacon, Lafayette, CO, USA), human PRC1 ON-TARGETplus SMART pool siRNA (L-019491-00-0020, Dharmacon), human custom-made Ndc80/Hec1 siRNA (oligo #1, sequence: 5'- GAAUUGCAGCAGACUAUUA-3', Dharmacon), human MISSION esiRNA kntc2 (NDC80) (oligo #2, EHU042171-20UG, Merck), human ON-TARGETplus SMART pool NUF2 siRNA (L-005289-00-000, Dharmacon), human custom-made 3'UTR HEC1 siRNA (oligo #3, Thermo Fisher Scientific; sequence 5′-CCCUGGGUCGUGUCAGGAA-3′), human ON-TARGETplus SMART pool KIFC1 (HSET) siRNA (L-004958-0010, Dharmacon), human KIF4A siRNA (sc-60888, Santa Cruz Biotechnology), human Kif18A siRNA (Ambion, #Cat 4390825, ID:s37882), human Kif22/Kid siRNA (Ambion, #Cat 4392420, ID:s7911), human WAPL ON-TARGETplus SMART pool siRNA (J-026287-10-0010, Dharmacon), human BUB1B/BuBR1 ON-TARGETplus SMART pool siRNA (L-004101-00-0005, Dharmacon, Lafayette, CO, USA), human Spindly siRNA (Sequence antisense: 5'- GAAAGGGUCUCAAACUGAA-3', dTdT overhangs, Sigma-Aldrich, St. Louis, MO, USA), and control siRNA (D-001810-10-05, Dharmacon, Lafayette, CO, USA).

*Drug treatments and drug washouts*

Aurora B inhibitor Barasertib (AZD1152-HQPA, Selleckchem, Munich, Germany, $IC_{50}$ value 0.32 nM) at a final concentration of 300 nM, was added acutely before imaging. CENP-E inhibitor GSK-923295 (MedChemExpress, Monmouth Junction, NJ, USA, IC50 value 3.2 nM) at a final concentration of 80 nM for RPE-1 and 200 nM for U2OS, to achieve the same effect, was added 1-4 hours before imaging in most experiments, or when noted acutely before imaging. Eg5 inhibitor Monastrol (HY-101071A/CS-6183, MedChemExpress, $IC_{50}$ value 50 μM) at a final concentration of 100 μM, was added 3 hours before imaging or acutely before imaging when noted. Aurora B inhibitor ZM-447439 (MedChemExpress, $IC_{50}$ value 130 nM) at a final concentration of 2 or 3 μM as noted, was added acutely before live imaging or 15 minutes before fixation as noted. Aurora A inhibitor MLN8237 (MedChemExpress, $IC_{50}$ value 4 nM) at a final final concentration of 125 nM or 250 nM as noted, was added acutely before imaging or 30-60 minutes before fixation. Bub1 inhibitor BAY-320 (MedChemExpress, $IC_{50}$ value 680 nM) at a final concentration of 10 μM, was added acutely before imaging. Haspin inhibitor 5-Iodotubercidin (5-ITu) (MedChemExpress, $IC_{50}$ value 5-9 nM) at a final concentration of 2 μM, was added acutely before imaging. Mps1 inhibitor AZ3146 (MedChemExpress, USA, $IC_{50}$ value 35 nM) at a final concentration of 500 nM, was added acutely before imaging. PLK1 inhibitor BI 2536 (MedChemExpress, $IC_{50}$ value 0.83 nM) at a final concentration of 100 nM, was added acutely before imaging. Inhibitor of PP1 and PP2A Okadaic acid (MedChemExpress, $IC_{50}$ value 0.1-0.3 nM for PP2A and 15-50 nM for PP1) at a final concentration of 1 μM, was added acutely before imaging or 30 minutes before washout of the CENP-E inhibitor as noted. Cytoplasmic dynein inhibitor Ciliobrevin D (MedChemExpress) at a final concentration of 20 μM, was added acutely before imaging. Proteasome inhibitor MG-132 (MedChemExpress, $IC_{50}$ value 100 nM) at a final concentration of 1 μM, was added acutely before imaging or together with CENP-E inhibitor as

noted. PLK4 inhibitor Centrinone (MedChemExpress, $K_i$ value 0.16 nM) at a final concentration of 300 nM, was added 1-5 days before the imaging as noted.

The stock solutions for all drugs were prepared in DMSO except Okadaic acid which was prepared in ethanol. The stock solutions of all drugs were kept aliquoted at 10-50 μL at -20 °C for a maximum period of three months or at -80 °C for a maximum period of six months. New aliquots were thawed weekly for each new experiment. All drugs were added to DMEM media used for cell culture to obtain the final concentration of a drug as described, except Ciliobrevin D, which was added to a serum-reduced Opti-MEM medium (Life Technologies, Waltham, MA, USA) that was placed on cells acutely before adding the drug, as Ciliobrevin D did not show any effect when used in DMEM medium with 10% FBS (Firestone *et al*, 2012). Drug washouts were performed by replacing drug-containing medium with 2 mL of fresh pre-warmed DMEM medium followed by four subsequent washouts with 2 mL of pre-warmed DMEM.

To deplete centrioles, Plk4 kinase activity was inhibited with centrinone, a small molecule inhibitor that blocks the centriole duplication cycle, and varied the duration of treatment to obtain spindles with different numbers of centrioles on each centrosome, a method established previously (Wong *et al*, 2015). Subsequently, we treated Plk4-inhibited cells with CENP-E inhibitor or DMSO and imaged cells a few hours after treatment using the same live cell imaging protocol described previously. Acute inhibition of Aurora B by ZM-447439 (2 or 3 μM) or barasertib (300 nM) induced premature anaphase onset 15-30 min after the addition of Aurora B inhibitor, as reported previously (Maia *et al*, 2010). Similarly, premature onset of anaphase was observed during the 30 min course of the imaging in cells acutely treated with the Mps1 inhibitor AZ3146 (500 nM), as expected from previous work (Santaguida *et al*, 2011). When noted in the text, we treated CENP-E inhibited cells with the proteasome inhibitor MG-132 together with Aurora B or Mps1 inhibitors to block premature anaphase onset. MG treatment provided more time for the chromosomes to complete the alignment successfully, as in the Aurora B inhibitor alone, anaphase ensued while some chromosomes were still in the alignment process.

Acute treatment of cells with dynein inhibitor 20 μM Ciliobrevin D splayed the spindle poles in all treated cells during 30 minutes after the addition of the drug, reflecting the reported role of the dynein-dynactin complex in the focus of the spindle poles in human cells (Firestone *et al*, 2012). Interestingly, co-inhibition of Bub1 by BAY-320 (10 μM) and Haspin by 5-ITu (2 μM) in some cells induced premature onset of anaphase during the first 20 minutes after addition of the drug, reflecting the possible role of both pathways in the maintenance of the spindle assembly checkpoint (Hengeveld *et al*, 2017). 30-minute long Okadaic acid treatment (1 μM) led to depolymerization of actin filaments and rounding of interphase cells (Fiorentini *et al*, 1996). Acute treatment of cells with Okadaic acid (1 uM) together with acute treatment with Aurora B inhibitor or after CENP-E inhibitor washout resulted in frequent expels of aligned kinetochores from the plate and sometimes complete breakage of the integrity of metaphase plates, but only after most of the polar chromosomes had already aligned to the plate, similar to previous reports of PP1 antibody injections into HeLa cells (Kim *et al*, 2010). After acute treatment of CENP-E inhibited cells with the Eg5 inhibitor monastrol (50 uM), spindles quickly shortened, as expected from previous reports (Vukušić *et al*, 2021). Similarly, acute and drastic spindle shortening was

observed in most CENP-E inhibited cells after acute addition of the Aurora A inhibitor MLN8237 (125 nM), as expected from previous studies (Ye *et al*, 2015). Acute inhibition of PLK1 by BI 2536 (100 nM) induced a fast block of spindle elongation and cytokinetic invasion in cells after the onset of anaphase observed only after CENP-E washout, as expected from previous reports (Petronczki *et al*, 2007).

Regarding cells imaged by confocal microscopy after the chronic inhibition of CENP-E by GSK-923295 (80 nM), all pseudo-metaphase spindles chosen for imaging were phenotypically similar between each other and between conditions where CENP-E was depleted or reactivated after washout of the CENP-E inhibitor: 1) in all cells few chromosomes were localized close to one of the spindle poles, called polar chromosomes, and their numbers ranged from 2-16 per cell; 2) occasionally in some cells few chromosomes were localized already in between spindle pole and equator; and 3) in all cells most chromosomes were already aligned and tightly packed at the metaphase plate. This type of chromosome arrangement was expected from previously published data that reported that only 10-30% of chromosomes upon NEBD require CENP-E-mediated alignment (Barisic *et al*, 2014). Likewise, under all conditions where CENP-E was perturbed and cells imaged by confocal microscopy during pseudo-metaphase, the overall displacement of spindle poles from each other was negligible (data not shown), consistent with cells being in a pseudo-metaphase state where there is no net change in spindle length. For LLSM-based assay, no inclusion criteria for imaging were used as the cells were non-synchronized and entered mitosis stochastically. Only randomly selected cells that entered mitosis and subsequently entered anaphase during imaging time were used for kinetochore and centrosome tracking analysis.

*Immunofluorescence*

For cell labeling with phopho-Knl1, phopho-Dsn1, phosphor-Hec1, phospho-Aurora A, phospho-Aurora B, phospho-AuroraA/B/C, and anti-Spindly antibodies, RPE-1 cells expressing CENP-A-GFP and centrin1-GFP grown on glass-bottom dishes (14 mm, No. 1.5, MatTek Corporation, Darmstadt, Germany) were pre-extracted with pre-warmed PEM buffer at 37 °C (0.1 M PIPES, 0.001 M MgCl2 × 6 H2O, 0.001 M EDTA, 0.5% Triton-X-100) for 30 s at room temperature and fixed by 1 ml of pre-warmed solution of 4% paraformaldehyde (PFA) for 20 min. All other antibodies were used on cells fixed for 2 minutes with ice-cold methanol, except for those used in STED microscopy, which are described below. After fixation, cells were washed 3 times for 5 min with 1 ml of PBS and permeabilized with 0.5% Triton-X-100 solution in water for 30 min at room temperature. To block unspecific binding, cells were incubated in 1 ml of blocking buffer (2% bovine serum albumin, BSA) for 2 h at room temperature. The cells were then washed 3 times for 5 min with 1 ml of PBS and incubated with 500 µl of primary antibody solution overnight at 4°C. Antibody incubation was performed using a blocking solution composed of 0.1% Triton, 1% BSA in PBS.

Following primary antibodies were used: rabbit monoclonal phopho-Knl1 (1.5 mg/ml, gift from J. Welburn, diluted 1:1000), rabbit monoclonal phopho-Dsn1 conjugated to Cy3 (0.5 mg/ml, gift from J. Welburn, diluted 1:250, diluted 1:500), rabbit monoclonal phospho-Aurora A (Thr288) (C39D8) (3079T, Cell Signalling Technology, diluted 1:500), rabbit monoclonal phospho-Aurora A (Thr288)/Aurora B (Thr232)/Aurora C (Thr198) (D12A11) (2914T, Cell Signalling

Technology, diluted 1:500), rabbit polyclonal phospho-Hec1 (Ser55) (GTX70017, GeneTex, diluted 1:500), rabbit polyclonal phospho-Aurora B (Thr232) (GTX85607, GeneTex, diluted 1:500), rabbit monoclonal Anti-NDC80 (HPA066330-100uL, Sigma-Aldrich, diluted 1:250), mouse monoclonal anti-KIFC1 (M-6, sc-100947, Santa Cruz, diluted 1:500), rabbit polyclonal anti-Kif18a (A301-080A, Bethyl Laboratories, diluted 1:500), mouse monoclonal anti-BubR1 (MAB3612, EMD Milipore, diluted 1:500), rabbit anti-Kif4A (A301-074A, Bethyl Laboratories, diluted 1:500), rabbit anti-SPINDLY/CCD98 (A301-354A, Bethyl Laboratories, dilued 1:500) and mouse monoclonal anti-KID (B-9, sc-390640, Santa Cruz, diluted 1:500).

After primary antibody, cells were washed in PBS and then incubated in 500 µL of secondary antibody solution for 1 h at room temperature. Following secondary antibodies were used: Donkey anti-rabbit IgG Alexa Fluor 647 (ab150075, Abcam, diluted 1:1000) for phopho-Dsn1, Donkey anti-rabbit IgG Alexa Fluor 594 (ab150064, Abcam, diluted 1:1000) for all other rabbit antibodies, Donkey anti-mouse IgG Alexa Fluor 594 (ab150108, Abcam, diluted, 1:1000) for all mouse antibodies except anti-KID which was conjugated with Donkey anti-mouse IgG Alexa Fluor 647 (ab150107, Abcam, diluted 1:1000). Finally, cells were washed with 1 ml of PBS, 3 times for 10 min. Cells were imaged either immediately following the imaging or were kept at 4°C before imaging for a maximum period of one week.

To visualize alpha-tubulin in STED resolution in the RPE-1 CENP-A-GFP centrin1-GFP cell line, the ice-cold methanol protocol was avoided because it destroyed the unstable fraction of microtubules (Ponjavić *et al*, 2021). Cells were washed with cell extraction buffer (CEB) and fixed with 3.2% paraformaldehyde (PFA) and 0.1% glutaraldehyde (GA) in PEM buffer (0.1 M PIPES, 0.001 M MgCl2 × 6 H2O, 0.001 M EGTA, 0.5% Triton-X-100) for 10 min at room temperature. After fixation with PFA and GA, for quenching, cells were incubated in 1 ml of freshly prepared 0.1% borohydride in PBS for 7 min and then in 1 mL of 100 mM $NH_4Cl$ and 100 mM glycine in PBS for 10 min at room temperature. To block nonspecific binding of antibodies, cells were incubated in 500 µL blocking/permeabilization buffer (2% normal goat serum and 0.5% Triton-X-100 in water) for 2 h at room temperature. Cells were then incubated in 500 µL of primary antibody solution containing rat anti-alpha-tubulin YL1/2 (MA1-80017, Invitrogen, CA, SAD, diluted 1:500) overnight at 4 °C. After incubation with a primary antibody, cells were washed 3 times for 10 min with 1 ml of PBS and then incubated with 500 µl of secondary antibody containing donkey anti-rat IgG Alexa Fluor 594 (ab150156, Abcam, diluted 1:300) for 2 h at room temperature, followed by wash with 1 ml of PBS 3 times for 10 min.

*Imaging*

Opterra I multipoint scanning confocal microscopy system (Bruker Nano Surfaces, Middleton, WI, USA) was mainly used for live-cell imaging of hTERT-RPE1 cells expressing CENP-A-GFP and Centrin1-GFP, in cells depleted of CENP-E by siRNAs and in cells with inhibited CENP-E by CENP-E inhibitor, in the assay we termed a confocal-based imaging assay. The system was mounted on a Nikon Ti-E inverted microscope equipped with a Nikon CFI Plan Apo VC 100x/1.4 numerical aperture oil objective (Nikon, Tokyo, Japan). The system was controlled with Prairie View Imaging Software (Bruker). During imaging, cells were kept at 37 ° C and at 5% $CO_2$ in the Okolab cage incubator (Okolab, Pozzuoli, NA, Italy). The laser power was set to 10% for the

488nm excitation laser. For optimal resolution and signal-to-noise ratio, a 60 µm pinhole aperture was used and the xy-pixel size was set to 83 nm. For excitation of GFP, a 488-nm diode laser line was used. The excitation light was separated from the emitted fluorescence using the Opterra dichroic and Barrier 488 eGFP filter set (Chroma, USA). Images were acquired with an Evolve 512 Delta Electron Multiplying Charge Coupled Device (EMCCD) camera (Photometrics, Tucson, AZ, USA) using a 150-ms exposure time and with a camera readout mode of 20 MHz. 30-60 z-stacks encompassing all focal planes with visible green signal were acquired with 0.5 µm spacing to cover the entire spindle area in depth with unidirectional xyz scan mode and with the "fast acquisition" option enabled in software. Images of six different cells were taken simultaneously every 30s-1 min. The total duration of the time-lapse movies was 30 min to 1 hour.

The STED confocal microscope system (Abberior Instruments) and the LSM800 laser scanning confocal system (Zeiss) were used for the remainder of the live-cell experiments we termed the confocal-based imaging assay and in hTERT-RPE1 cells expressing CENP-A-mCerulean and Mad2-mRuby after reactivation of CENP-E activity. STED microscopy was also used to image all fixed cells in super-resolution. STED microscopy was performed using an Expert Line easy3D STED microscope system (Abberior Instruments, Göttingen, Germany) with the 100 x/1.4NA UPLSAPO100x oil objective (Olympus, Tokio, Japan) and an avalanche photodiode detector (APD). The 488 nm line was used for excitation, with the addition of the 561 nm line for excitation and the 775 nm laser line for depletion during STED super-resolution imaging. The images were acquired using Imspector software. The xy pixel size for fixed cells was 20 nm and 10 focal planes were acquired with a 300 nm distance between the planes. For confocal live cell imaging of cells, the xy pixel size was 80 nm and 16 focal images were acquired, with 0.5 µm distance between the planes and 1 min time intervals between different frames. During imaging, live cells were kept at 37 ° C and at 5% $CO_2$ in the Okolab stage incubation chamber system (Okolab, Pozzuoli, NA, Italy).

LSM 800 confocal system (Zeiss) was used for the rest of live-cell confocal-based imaging in hTERT-RPE1 cells expressing CENP-A-GFP and centrin1-GFP with the following parameters: sampling in xy, 0.27 µm; z step size, 0.5 µm; total number of slices, 32; pinhole, 48.9 µm; unidirectional scan speed, 10; averaging, 2; 63x Oil DIC f/ELYRA objective (1.4 NA), 488 nm laser line (0.1% power), and detection ranges of 410–558 nm. Images were acquired using ZEN 2.6 (blue edition; Zeiss). Six cells in volumes of 15 µm were imaged sequentially every 1 minute at different positions determined right after the addition of a drug. During imaging, cells were incubated at 37 °C and 5% $CO_2$ using a Pecon stage incubation chamber system (Pecon, Heating Insert P S1, #130-800 005). The system was also used for imaging of all other fixed cells that were not imaged by STED microscopy, on multiples positions and at the confocal lateral resolution.

The Lattice Lightsheet 7 system (Zeiss) was used for live cell imaging of hTERT-RPE1 cells expressing CENP-A-GFP and Centrin1-GFP and U2OS cells expressing CENP-A-GFP after reactivation of CENP-E activity, in cells depleted of CENP-E by siRNAs and in cells with inhibited CENP-E by CENP-E inhibitor, in assay we called LLSM-based imaging assay. The system was equipped with an illumination objective lens 13.3×/0.4 (at a 30° angle to cover the glass) with a static phase element and a detection objective lens 44.83×/1.0 (at a 60° angle to cover the glass)

with an Alvarez manipulator. The automatic immersion of water was applied from the motorized dispenser at an interval of 20 or 30 minutes. Right after sample mounting, four steps of the 'create immersion' auto immersion option were applied. The sample was illuminated with a 488-nm diode laser (power output 10 Mw) with laser power set to 1-2%. The detection module consisted of a Hamamatsu ORCA-Fusion sCMOS camera with exposure time set to 15-20 ms. The LBF 405/488/561/642 emission filter was used. During imaging, cells were kept at 37 °C and at 5% CO2 in a Zeiss stage incubation chamber system (Zeiss). The width of the imaging area in the x dimension was set from 1 to 1.5 mm.

*Tracking of centrosomes and kinetochores*

The spatial x and y coordinates of the kinetochore pairs were extracted in each time frame using the Low Light Tracking Tool (v.0.10), an ImageJ plugin based on the Nested Maximum Likelihood Algorithm, as previously described(Vukušić *et al*, 2021). Tracking of polar kinetochores in the x and y planes was performed on the maximum intensity projections of all acquired z planes. Some kinetochore pairs could not be successfully tracked in all frames, mainly owing to cell and spindle movements in the z-direction over time. Spindle poles were manually tracked with points placed between the center of the two centrioles or centriole in centrinone treated cells. Kinetochore pairs that were aligned at the start of the imaging in a confocal-based imaging assay were also manually tracked in two dimensions. Quantitative analysis of all parameters was performed using custom-made MATLAB scripts (MatlabR2021a 9.10.0) scripts.

Due to the inability to reliably track polar kinetochores across all time frames due to neighboring kinetochores, tracking of polar kinetochores routinely commenced a few frames before the kinetochore pair began moving towards the equatorial plane. In the CENP-E reactivation assay, kinetochores were tracked from the onset of imaging until the successful identification of the same kinetochore pair, which occurred when the kinetochore pair was lost in the imaging plane, among other kinetochores, or when the imaging session ended, whichever came first. Aligned kinetochore pairs were tracked in the confocal-based assay using the same protocol.

*Quantification of mean Mad2, pHec1, pKnl1, pAurora A, pAuroraB intensities of kinetochore pairs*

The fluorescence intensity signal of each kinetochore in both CENP-A and respective kinetochore protein channel (Mad2, pDsn1, pKnl1) was measured by using the "*Oval selection*" tool in ImageJ with the size and position defined by the borders of the CENP-A signal of each kinetochore in the sum intensity projection of all acquired z-planes. pAurora A signal was measured using the "*Oval selection*" tool around the centriole signal as the center or around the signal of the Aurora A of the same size on the pole without centriole. The background fluorescence intensity measured in the cytoplasm was subtracted from the obtained values, and the calculated integrated intensity value was divided by the number of z-stacks used to generate the sum projection of each cell. The obtained mean intensity value subtracted for background for each kinetochore was normalized to the intensity of the CENP-A signal. For the pHec1 labeling experiments, the mean signal of Hec1 and CENP-A was measured by the same approach but on one z-plane where kinetochore CENP-A signal was the highest. The mean signal of the pAurora B was measured between extent of

CENP-A signals of sister kinetochore pairs, and the mean value was normalized to mean value of CENP-A signal of each sister kinetochore pair. All movies used for the analysis were performed using the same fixation protocol and were imaged with the same imaging parameters in at least three independent biological replicates. To avoid measurement of non-specific labeling of the spindle poles that are known artefacts of phospho-antibodies to kinetochore proteins (pAurB, pKnl1, pHec1) (Welburn *et al*, 2010), only the kinetochores outside of the circular pole signal (~1 μm from the centrosome) were measured and used for analysis.

*Quantification of mean signal intensities of proteins after RNAi interreference and Mad2 after CENP-E perturbations*

The fluorescence intensity signals were measured in triplicate samples for targeting and non-targeting groups for each siRNA treatment. Each siRNA targeting and non-targeting triplicates were imaged by the same protocol. All proteins were measured in mitotic cells at their respective locations during mitosis by using the "*Polygon selection tool*", as established by many previous studies: kinetochores and chromosomes defined by the DAPI or CENP-A area on sum projection for CENP-E, Mad2, Spindly, BubR1, and on single planes for Hec1 defined by the CENP-A signal; entire spindle region defined by extent of centrin-1 and CENP-A signals on sum projections for Kif4a, Kif18a, and HSET; and chromosomes defined by DAPI signal on sum projections for Kid.

*Quantification of polar kinetochore pairs*

Polar kinetochores in all experiments were defined as kinetochore pairs that are closer to one of the spindle poles than to the equatorial plane. In confocal-based experiments polar chromosomes were defined from the onset of imaging. The number of polar kinetochore pairs in cells that were imaged from the onset of mitosis, mainly related to LLSM-based experiments, was quantified 12 minutes from the onset of mitosis and then every 6 minutes until the onset of anaphase or until the end of the imaging on maximum intensity projections of all acquired z planes. In cells treated with centrinone and their respective DMSO controls, the number of polar chromosomes was measured in time when the spindle finished the bipolarization process, e.g., the elongation of the spindle. This was done because all spindles of the 1:0 type with only one centriole at the beginning of mitosis went into the monopolar state and stayed in this state for variable durations before bipolarization, ranging from 10 to 50 minutes, as reported previously (Dudka *et al*, 2019). The residence time of polar chromosomes on spindle poles was defined as a time from spindle bipolarization until the last polar entered the metaphase plate, or a cell entered anaphase with uncongressed polar chromosome. Duration of mitosis was defined as the time from the first signs of nuclear envelope breakdown to one frame before visible onset of anaphase defined by the separation of sister kinetochore pairs.

To calculate the distance between kinetochores in fixed samples, two points were placed at the center of the signal in each pair of kinetochores using a 'Point tool' in ImageJ. Congression velocity was calculated for each pair of kinetochores in the last 6 minutes (RPE-1) or 4 minutes (U2OS) before the center of the pair of kinetochores surpassed 2 μm from the equatorial plane measured as the nearest distance from a center of a pair to a plane. These times represent the fast kinetochore movement towards the plate. The different time for calculation of velocities between

the cell lines was chosen due to faster congression in U2OS, thus polar chromosomes spend less time in movement compared to RPE-1. Aligned kinetochore pair was defined as every pair that was found 3 μm from the equatorial plane at any given time. The equatorial or metaphase plane was defined in each time frame as the line perpendicular to the line connecting the centrosomes at their midpoint. The angle between the kinetochore pairs and the main spindle axis was defined as an angle between a line connecting two centrosomes and a line connecting the center of the kinetochore pair and a spindle pole nearest to the respective pair.

Three types of mitotic outcomes were analyzed in CENP-E-depleted anaphase spindles in RPE-1 and U2OS cells: persistent polar kinetochores, repaired polar kinetochores, and death in mitosis. Cells classified as 'mis-segregated as polar' were defined as those in which kinetochores were situated outside the metaphase plate after spindle bipolarization and persisted there after the onset of anaphase. Cells classified as 'aligned before anaphase' were defined as those in which kinetochores were situated outside the metaphase plate after spindle bipolarization but aligned to the metaphase plate before anaphase onset. Cells classified as 'death' were defined as those in which kinetochores were situated outside the metaphase plate after spindle bipolarization while the cell subsequently did not enter anaphase, but instead showed signs of apoptotic blebbing and rapid disintegration of the CENP-A signal.

In images acquired using STED microscopy, lateral attachments were defined as those in which the kinetochore did not form visible attachments with microtubules that terminate at the kinetochore, defined by the CENP-A signal; end-on attachments were defined as those in which the kinetochore formed visible attachments with microtubules that terminated at the kinetochore, defined by the CENP-A signal, with no visible microtubule signal just below or above the kinetochore. In Figure panels 3C and 3G, alignment was considered successful if a chromosome, initially polar at the beginning of imaging, moved to within 2 μm of the equatorial plane after 30 minutes. The 30-minute period was chosen because it represents the minimum imaging time used for the confocal-based microscopy assay, and it covers the majority of the imaged cells.

The alignment categories in Figure 3I were defined as follows: "No metaphase plate" indicated that no metaphase plate is formed. "High misalignment" indicated a metaphase plate is formed, but more than 5 chromosomes are outside the plate. "Low misalignment" indicated a situation where a metaphase plate is formed, with fewer than 5 chromosomes outside the plate. Finally, "Tight metaphase plate" signified the formation of a tight metaphase plate with no chromosome misalignment. "Maximum spread of chromosomes" was measured on maximum intensity projections as the nearest distance between centers of two most separated kinetochore pairs.

*Image processing and statistical analysis*

Image processing was performed in ImageJ (National Institutes of Health, Bethesda, MD, USA). Quantification and statistical analysis were performed in MatLab. The figures were assembled in Adobe Illustrator CS6 and Adobe Photoshop CS6 (Adobe Systems, Mountain View, CA, USA). Raw images were used for quantification. The images of spindles were rotated in every frame to fit the long axis of the spindle to be parallel with the central long axis of the box in ImageJ and the spindle short axis to be parallel with the central short axis of the designated box in ImageJ. The

designated box sizes were cut to the same dimensions for all panels in the figures where the same experimental setups were used across the treatments. When comparing different treatments in channels in which the same protein was labeled, the minimum and maximum intensity of that channel was set to the values in the control treatment. When indicated, the smoothing of the images was performed using the "Gaussian blur" function in ImageJ (s=0.5-1.0). Colour-coded maximum intensity projections of the z-stacks were done using the "*Temporal colour code*" tool in Fiji by applying “16-color” or “Spectrum” lookup-table (LUT) or other LUT as indicated. For the generation of univariate scatter plots, the open Matlab extension "UnivarScatter" was used (https://github.com/manulera/UnivarScatter).

Data are given as mean ± standard deviation (s.t.d.), unless otherwise stated. The mean line was plotted to encompass a minimum of 60% of the data points for each treatment. Other dispersion measures used are defined in their respective figure captions or in Figure 1 and Appendix Figure S1 if the same measures are used across all figures. The exact values of n are given in the respective figure captions, where n represents the number of cells or the number of tracked kinetochore pairs, as defined for each n in the figure captions or tables. The number of independent biological replicates is also given in the figure captions. An independent experiment for acute drug treatments was defined by the separate addition of a drug to a population of cells in a dish. The number of cells imaged simultaneously ranged from 1 to 7, depending on the specific microscopy system used. The p values when comparing multiple classes were obtained using the one-way ANOVA test followed by Tukey's Honest Significant Difference (HSD) test (significance level was 5%). $p < 0.05$ was considered statistically significant, very significant if $0.001 < p < 0.01$ and extremely significant if $p < 0.001$. Values of all significant differences are given with the degree of significance indicated ($*0.01 < p < 0.05$, $**0.001 < p < 0.01$, $***p < 0.001$, $**** < 0.0001$). For the linear regression correlation measure between two parameters, the nonparametric Spearman correlation coefficient, termed rs, was used where $p<0.001$, calculated using the 'corr' function in Matlab (Statistics Toolbox R14). No statistical methods were used to predetermine the sample size. The experiments were not randomized and, except where stated, the investigators were not blinded to allocation during experiments and outcome evaluation.

## REFERENCES


Ali A & Stukenberg PT (2023) Aurora kinases: Generators of spatial control during mitosis. *Front Cell Dev Biol* 11: 265

Auckland P & McAinsh AD (2015) Building an integrated model of chromosome congression. *J Cell Sci* 128: 3363–3374

Bakhoum SF, Genovese G & Compton DA (2009) Deviant kinetochore microtubule dynamics underlie chromosomal instability. *Curr Biol* 19: 1937–1942

Bancroft J, Auckland P, Samora CP & McAinsh AD (2015) Chromosome congression is promoted by CENP-Q- and CENP-Edependent pathways. *J Cell Sci* 128: 171–184

Barisic M, Aguiar P, Geley S & Maiato H (2014) Kinetochore motors drive congression of peripheral polar chromosomes by overcoming random arm-ejection forces. *Nat Cell Biol* 16: 1249–1256

Barisic M & Maiato H (2015) Dynein prevents erroneous kinetochore-microtubule attachments in mitosis. *Cell Cycle* 14: 3356

Barisic M, Silva E Sousa R, Tripathy SK, Magiera MM, Zaytsev A V., Pereira AL, Janke C, Grishchuk EL & Maiato H (2015) Microtubule detyrosination guides chromosomes during mitosis. *Science (80- )* 348: 799–803

Barisic M, Sohm B, Mikolcevic P, Wandke C, Rauch V, Ringer T, Hess M, Bonn G & Geley S (2010) Spindly/CCDC99 is required for efficient chromosome congression and mitotic checkpoint regulation. *Mol Biol Cell* 21: 1968–1981

Broad AJ, DeLuca KF & DeLuca JG (2020) Aurora B kinase is recruited to multiple discrete kinetochore and centromere regions in human cells. *J Cell Biol* 219

Cai S, O'Connell CB, Khodjakov A & Walczak CE (2009) Chromosome congression in the absence of kinetochore fibres. *Nat Cell Biol* 11: 832–838

Cane S, Ye AA, Luks-Morgan SJ & Maresca TJ (2013) Elevated polar ejection forces stabilize kinetochore-microtubule attachments. *J Cell Biol* 200: 203–218

Cheerambathur DK, Gassmann R, Cook B, Oegema K & Desai A (2013) Crosstalk between microtubule attachment complexes ensures accurate chromosome segregation. *Science (80- )* 342: 1239–1242

Cheeseman IM, Chappie JS, Wilson-Kubalek EM & Desai A (2006) The Conserved KMN Network Constitutes the Core Microtubule-Binding Site of the Kinetochore. *Cell* 127: 983–997

Chen RH, Waters JC, Salmon ED & Murray AW (1996) Association of spindle assembly checkpoint component XMAD2 with unattached kinetochores. *Science (80- )* 274: 242–246

Cmentowski V, Ciossani G, d'Amico E, Wohlgemuth S, Owa M, Dynlacht B & Musacchio A (2023) RZZ-Spindly and CENP-E form an integrated platform to recruit dynein to the kinetochore corona. *EMBO J* 42

Collin P, Nashchekina O, Walker R & Pines J (2013) The spindle assembly checkpoint works like a rheostat rather than a toggle switch. *Nat Cell Biol* 15: 1378–1385

Cooke CA, Schaar B, Yen TJ & Earnshaw WC (1997) Localization of CENP-E in the fibrous corona and outer plate of mammalian kinetochores from prometaphase through anaphase. *Chromosoma* 106: 446–455

Dai J, Sultan S, Taylor SS & Higgins JMG (2005) The kinase haspin is required for mitotic histone H3 Thr 3 phosphorylation and normal metaphase chromosome alignment. *Genes Dev* 19: 472–488

DeLuca JG, Gall WE, Ciferri C, Cimini D, Musacchio A & Salmon ED (2006) Kinetochore Microtubule Dynamics and Attachment Stability Are Regulated by Hec1. *Cell* 127: 969–982

DeLuca KF, Lens SMA & DeLuca JG (2011) Temporal changes in Hec1 phosphorylation control kinetochore–microtubule attachment stability during mitosis. *J Cell Sci* 124: 622–634

Ditchfield C, Johnson VL, Tighe A, Ellston R, Haworth C, Johnson T, Mortlock A, Keen N & Taylor SS (2003) Aurora B couples chromosome alignment with anaphase by targeting BubR1, Mad2, and Cenp-E to kinetochores. *J Cell Biol* 161: 267–280

Drpic D, Pereira AJ, Barisic M, Maresca TJ & Maiato H (2015) Polar Ejection Forces Promote the Conversion from Lateral to End-on Kinetochore-Microtubule Attachments on Mono-oriented Chromosomes. *Cell Rep* 13: 460–468

Dudka D, Castrogiovanni C, Liaudet N, Vassal H & Meraldi P (2019) Spindle-Length-Dependent HURP Localization Allows Centrosomes to Control Kinetochore-Fiber Plus-End Dynamics. *Curr Biol* 29: 3563-3578.e6

Ehlén Å, Martin C, Miron S, Julien M, Theillet FX, Ropars V, Sessa G, Beaurepere R, Boucherit V, Duchambon P, *et al* (2020) Proper chromosome alignment depends on BRCA2 phosphorylation by PLK1. *Nat Commun 2020 111* 11: 1–21

Eibes S, Rajendraprasad G, Guasch-Boldu C, Kubat M, Steblyanko Y & Barisic M (2023) CENP-E activation by Aurora A and B controls kinetochore fibrous corona disassembly. *Nat Commun 2023 141* 14: 1–14

Ertych N, Stolz A, Stenzinger A, Weichert W, Kaulfuß S, Burfeind P, Aigner A, Wordeman L & Bastians H (2014) Increased microtubule assembly rates influence chromosomal instability in colorectal cancer cells. *Nat Cell Biol* 16: 779–791

Etemad B, Kuijt TEF & Kops GJPL (2015) Kinetochore–microtubule attachment is sufficient to satisfy the human spindle assembly checkpoint. *Nat Commun 2015 61* 6: 1–8

Famulski JK & Chan GK (2007) Aurora B kinase-dependent recruitment of hZW10 and hROD to tensionless kinetochores. *Curr Biol* 17: 2143–2149

Fiorentini C, Matarrese P, Fattorossi A & Donelli G (1996) Okadaic acid induces changes in the organization of F-actin in intestinal cells. *Toxicon* 34: 937–945

Firestone AJ, Weinger JS, Maldonado M, Barlan K, Langston LD, O'Donnell M, Gelfand VI, Kapoor TM & Chen JK (2012) Small-molecule inhibitors of the AAA+ ATPase motor cytoplasmic dynein. *Nature* 484: 125–129

Gassmann R (2023) Dynein at the kinetochore. *J Cell Sci* 136

Gassmann R, Holland AJ, Varma D, Wan X, Çivril F, Cleveland DW, Oegema K, Salmon ED & Desai A (2010) Removal of Spindly from microtubule-attached kinetochores controls spindle checkpoint silencing in human cells. *Genes Dev* 24: 957–971

Gliech CR, Yeow ZY, Tapias-Gomez D, Yang Y, Huang Z, Tijhuis AE, Spierings DCJ, Foijer F, Chung G, Tamayo N, *et al* (2024) Weakened APC/C activity at mitotic exit drives cancer vulnerability to KIF18A inhibition. *EMBO J* 43: 666–694

Gomes AM, Orr B, Novais-Cruz M, De Sousa F, Macário-Monteiro J, Lemos C, Ferrás C & Maiato H (2022) Micronuclei from misaligned chromosomes that satisfy the spindle assembly checkpoint in cancer cells. *Curr Biol* 32: 4240-4254.e5

Gudimchuk N, Vitre B, Kim Y, Kiyatkin A, Cleveland DW, Ataullakhanov FI & Grishchuk EL (2013) Kinetochore kinesin CENP-E is a processive bi-directional tracker of dynamic microtubule tips. *Nat Cell Biol* 15: 1079–1088

Hadders MA, Hindriksen S, Truong MA, Mhaskar AN, Pepijn Wopken J, Vromans MJM & Lens SMA (2020) Untangling the contribution of Haspin and Bub1 to Aurora B function during mitosis. *J Cell Biol* 219

Hengeveld RCC, Vromans MJM, Vleugel M, Hadders MA & Lens SMA (2017) Inner centromere localization of the CPC maintains centromere cohesion and allows mitotic checkpoint silencing. *Nat Commun* 8

Hindriksen S, Lens SMA & Hadders MA (2017) The ins and outs of Aurora B inner centromere localization. *Front Cell Dev Biol* 5: 112

Huang Y, Lin L, Liu X, Ye S, Yao PY, Wang W, Yang F, Gao X, Li J, Zhang Y, *et al* (2019) BubR1 phosphorylates CENP-E as a switch enabling the transition from lateral association to end-on capture of spindle microtubules. *Cell Res* 29: 562

Iemura K & Tanaka K (2015) Chromokinesin Kid and kinetochore kinesin CENP-E differentially support chromosome congression without end-on attachment to microtubules. *Nat Commun* 6

Kabeche L & Compton DA (2013) Cyclin A regulates kinetochore microtubules to promote faithful chromosome segregation. *Nature* 502: 110–113

Kajtez J, Solomatina A, Novak M, Polak B, Vukušić K, Rüdiger J, Cojoc G, Milas A, Šumanovac Šestak I, Risteski P, *et al* (2016) Overlap microtubules link sister k-fibres and balance the forces on bi-oriented kinetochores. *Nat Commun* 7

Kapoor TM, Lampson MA, Hergert P, Cameron L, Cimini D, Salmon ED, McEwen BF & Khodjakov A (2006) Chromosomes can congress to the metaphase plate before biorientation. *Science (80- )* 311: 388–391

Kapoor TM, Mayer TU, Coughlin ML & Mitchison TJ (2000) Probing spindle assembly mechanisms with monastrol, a small molecule inhibitor of the mitotic kinesin, Eg5. *J Cell Biol* 150: 975–988

Kawashima SA, Tsukahara T, Langegger M, Hauf S, Kitajima TS & Watanabe Y (2007) Shugoshin enables tension-generating attachment of kinetochores by loading Aurora to centromeres. *Genes Dev* 21: 420–435

Kim Y, Heuser JE, Waterman CM & Cleveland DW (2008) CENP-E combines a slow, processive motor and a flexible coiled coil to produce an essential motile kinetochore tether. *J Cell Biol* 181: 411–419

Kim Y, Holland AJ, Lan W & Cleveland DW (2010) Aurora kinases and protein phosphatase 1 mediate chromosome congression through regulation of CENP-E. *Cell* 142: 444–455

Klaasen SJ, Truong MA, van Jaarsveld RH, Koprivec I, Štimac V, de Vries SG, Risteski P, Kodba S, Vukušić K, de Luca KL, *et al* (2022) Nuclear chromosome locations dictate segregation error frequencies. *Nature* 607: 604–609

Kops GJPL & Gassmann R (2020) Crowning the Kinetochore: The Fibrous Corona in Chromosome Segregation. *Trends Cell Biol* 30: 653–667

Kruse T, Zhang G, Larsen MSY, Lischetti T, Streicher W, Nielsen TK, Bjørn SP & Nilsson J (2013) Direct binding between BubR1 and B56-PP2A phosphatase complexes regulate mitotic progression. *J Cell Sci* 126: 1086–1092

Kuhn J & Dumont S (2017) Spindle assembly checkpoint satisfaction occurs via end-on but not lateral attachments under tension. *J Cell Biol* 216: 1533–1542

Lampson MA & Kapoor TM (2005) The human mitotic checkpoint protein BubR1 regulates chromosome-spindle attachments. *Nat Cell Biol* 7: 93–98

Lampson MA, Renduchitala K, Khodjakov A & Kapoor TM (2004) Correcting improper chromosome-spindle attachments during cell division. *Nat Cell Biol* 6: 232–237

Legal T, Hayward D, Gluszek-Kustusz A, Blackburn EA, Spanos C, Rappsilber J, Gruneberg U & Welburn JPI (2020) The C-terminal helix of BubR1 is essential for CENP-E-dependent chromosome alignment. *J Cell Sci* 133

Lončarek J, Kisurina-Evgenieva O, Vinogradova T, Hergert P, La Terra S, Kapoor TM & Khodjakov A (2007) The centromere geometry essential for keeping mitosis error free is controlled by spindle forces. *Nat 2007 4507170* 450: 745–749

Magidson V, O'Connell CB, Lončarek J, Paul R, Mogilner A & Khodjakov A (2011) The spatial arrangement of chromosomes during prometaphase facilitates spindle assembly. *Cell* 146: 555–567

Maia AF, Feijão T, Vromans MJM, Sunkel CE & Lens SMA (2010) Aurora B kinase cooperates with CENP-E to promote timely anaphase onset. *Chromosoma* 119: 405–413

Maiato H, Gomes AM, Sousa F & Barisic M (2017) Mechanisms of Chromosome Congression during Mitosis. *Biol 2017, Vol 6, Page 13* 6: 13

Mao Y, Desai A & Cleveland DW (2005) Microtubule capture by CENP-E silences BubR1-dependent mitotic checkpoint signaling. *J Cell Biol* 170: 873–880

Matković J, Ghosh S, Ćosić M, Eibes S, Barišić M, Pavin N & Tolić IM (2022) Kinetochore- and chromosome-driven transition of microtubules into bundles promotes spindle assembly. *Nat Commun* 13

McAinsh AD & Kops GJPL (2023) Principles and dynamics of spindle assembly checkpoint signalling. *Nat Rev Mol Cell Biol* 24: 543–559

McEwen BF, Chan GKT, Zubrowski B, Savoian MS, Sauer MT & Yen TJ (2001) CENP-E is essential for reliable bioriented spindle attachment, but chromosome alignment can be achieved via redundant mechanisms in mammalian cells. *Mol Biol Cell* 12: 2776–2789

McEwen BF, Heagle AB, Cassels GO, Buttle KF & Rieder CL (1997) Kinetochore fiber maturation in PtK1 cells and its implications for the mechanisms of chromosome congression and anaphase onset. *J Cell Biol* 137: 1567–1580

Navarro AP & Cheeseman IM (2021) Kinetochore assembly throughout the cell cycle. *Semin Cell Dev Biol* 117: 62–74

Petronczki M, Glotzer M, Kraut N & Peters JM (2007) Polo-like kinase 1 triggers the initiation of cytokinesis in human cells by promoting recruitment of the RhoGEF Ect2 to the central spindle. *Dev Cell* 12: 713–725

Polak B, Risteski P, Lesjak S & Tolić IM (2017) PRC1-labeled microtubule bundles and kinetochore pairs show one-to-one association in metaphase. *EMBO Rep* 18: 217–230

Ponjavić I, Vukušić K & Tolić IM (2021) Expansion microscopy of the mitotic spindle. *Methods Cell Biol* 161: 247–274

Quinton RJ, DiDomizio A, Vittoria MA, Kotýnková K, Ticas CJ, Patel S, Koga Y, Vakhshoorzadeh J, Hermance N, Kuroda TS, *et al* (2021) Whole-genome doubling confers unique genetic vulnerabilities on tumour cells. *Nature* 590: 492–497

Renda F, Miles C, Tikhonenko I, Fisher R, Carlini L, Kapoor TM, Mogilner A & Khodjakov A (2022) Non-centrosomal microtubules at kinetochores promote rapid chromosome biorientation during mitosis in human cells. *Curr Biol*

Risteski P, Božan D, Jagrić M, Bosilj A, Pavin N & Tolić IM (2022) Length-dependent poleward flux of sister kinetochore fibers promotes chromosome alignment. *Cell Rep* 40

Sacristan C, Ahmad MUD, Keller J, Fermie J, Groenewold V, Tromer E, Fish A, Melero R, Carazo JM, Klumperman J, *et al* (2018) Dynamic kinetochore size regulation promotes microtubule capture and chromosome biorientation in mitosis. *Nat Cell Biol 2018 207* 20: 800–810

Salimian KJ, Ballister ER, Smoak EM, Wood S, Panchenko T, Lampson MA & Black BE (2011) Feedback control in sensing chromosome biorientation by the Aurora B kinase. *Curr Biol* 21: 1158–1165

Santaguida S, Vernieri C, Villa F, Ciliberto A & Musacchio A (2011) Evidence that Aurora B is

implicated in spindle checkpoint signalling independently of error correction. *EMBO J* 30: 1508–1519

Schaar BT, Chan GKT, Maddox P, Salmon ED & Yen TJ (1997) CENP-E function at kinetochores is essential for chromosome alignment. *J Cell Biol* 139: 1373–1382

Shrestha RL, Conti D, Tamura N, Braun D, Ramalingam RA, Cieslinski K, Ries J & Draviam VM (2017) Aurora-B kinase pathway controls the lateral to end-on conversion of kinetochore-microtubule attachments in human cells. *Nat Commun* 8

Shrestha RL & Draviam VM (2013) Lateral to end-on conversion of chromosome-microtubule attachment requires kinesins cenp-e and MCAK. *Curr Biol* 23: 1514–1526

Song X, Conti D, Shrestha RL, Braun D & Draviam VM (2021) Counteraction between Astrin-PP1 and Cyclin-B-CDK1 pathways protects chromosome-microtubule attachments independent of biorientation. *Nat Commun* 12

Stumpff J, von Dassow G, Wagenbach M, Asbury C & Wordeman L (2008) The Kinesin-8 Motor Kif18A Suppresses Kinetochore Movements to Control Mitotic Chromosome Alignment. *Dev Cell* 14: 252–262

Su KC, Barry Z, Schweizer N, Maiato H, Bathe M & Cheeseman IMP (2016) A Regulatory Switch Alters Chromosome Motions at the Metaphase-to-Anaphase Transition. *Cell Rep* 17: 1728–1738

Suijkerbuijk SJE, van Dam TJP, Karagöz GE, von Castelmur E, Hubner NC, Duarte AMS, Vleugel M, Perrakis A, Rüdiger SGD, Snel B, *et al* (2012) The Vertebrate Mitotic Checkpoint Protein BUBR1 Is an Unusual Pseudokinase. *Dev Cell* 22: 1321–1329

Taveras C, Liu C & Mao Y (2019) A tension-independent mechanism reduces Aurora B-mediated phosphorylation upon microtubule capture by CENP-E at the kinetochore. *Cell Cycle* 18: 1349

Tovini L & McClelland SE (2019) Impaired CENP-E Function Renders Large Chromosomes More Vulnerable to Congression Failure. *Biomol 2019, Vol 9, Page 44* 9: 44

Tucker JB, Bonema SC, García-Varela R, Denu RA, Hu Y, McGregor SM, Burkard ME & Weaver BA (2023) Misaligned Chromosomes are a Major Source of Chromosomal Instability in Breast Cancer. *Cancer Res Commun* 3: 54–65

Valdez VA, Neahring L, Petry S & Dumont S (2023) Mechanisms underlying spindle assembly and robustness. *Nat Rev Mol Cell Biol* 24: 523–542

Vasquez-Limeta A & Loncarek J (2021) Human centrosome organization and function in interphase and mitosis. *Semin Cell Dev Biol* 117: 30–41

Vukušić K, Ponjavić I, Buđa R, Risteski P & Tolić IM (2021) Microtubule-sliding modules based on kinesins EG5 and PRC1-dependent KIF4A drive human spindle elongation. *Dev Cell* 56: 1253-1267.e10

Vukušić K & Tolić IM (2022) Polar Chromosomes-Challenges of a Risky Path. *Cells* 11

Walczak CE, Cai S & Khodjakov A (2010) Mechanisms of chromosome behaviour during

mitosis. *Nat Rev Mol Cell Biol* 11: 91–102

Weaver BAA, Bonday ZQ, Putkey FR, Kops GJPL, Silk AD & Cleveland DW (2003) Centromere-associated protein-E is essential for the mammalian mitotic checkpoint to prevent aneuploidy due to single chromosome loss. *J Cell Biol* 162: 551–563

Weber J, Legal T, Lezcano AP, Gluszek-Kustusz A, Paterson C, Eibes S, Barisic M, Davies OR & Welburn JPI (2024) A conserved CENP-E region mediates BubR1-independent recruitment to the outer corona at mitotic onset. *Curr Biol* 34: 1133-1141.e4

Welburn JPI, Vleugel M, Liu D, Yates JR, Lampson MA, Fukagawa T & Cheeseman IM (2010) Aurora B Phosphorylates Spatially Distinct Targets to Differentially Regulate the Kinetochore-Microtubule Interface. *Mol Cell* 38: 383–392

Wong YL, Anzola J V., Davis RL, Yoon M, Motamedi A, Kroll A, Seo CP, Hsia JE, Kim SK, Mitchell JW, *et al* (2015) Reversible centriole depletion with an inhibitor of Polo-like kinase 4. *Science* 348: 1155

Wood KW, Lad L, Luo L, Qian X, Knight SD, Nevins N, Brejc K, Sutton D, Gilmartin AG, Chua PR, *et al* (2010) Antitumor activity of an allosteric inhibitor of centromere-associated protein-E. *Proc Natl Acad Sci U S A* 107: 5839–5844

Wu J, Larreategui-Aparicio A, Lambers MLA, Bodor DL, Klaasen SJ, Tollenaar E, de Ruijter-Villani M & Kops GJPL (2023) Microtubule nucleation from the fibrous corona by LIC1-pericentrin promotes chromosome congression. *Curr Biol* 33

Yang J, Ikezoe T, Nishioka C, Tasaka T, Taniguchi A, Kuwayama Y, Komatsu N, Bandobashi K, Togitani K, Koeffler HP, *et al* (2007) AZD1152, a novel and selective aurora B kinase inhibitor, induces growth arrest, apoptosis, and sensitization for tubulin depolymerizing agent or topoisomerase II inhibitor in human acute leukemia cells in vitro and in vivo. *Blood* 110: 2034–2040

Yao X, Anderson KL & Cleveland DW (1997) The microtubule-dependent motor centromere-associated protein E (CENP-E) is an integral component of kinetochore corona fibers that link centromeres to spindle microtubules. *J Cell Biol* 139: 435–447

Ye AA, Deretic J, Hoel CM, Hinman AW, Cimini D, Welburn JP & Maresca TJ (2015) Aurora A Kinase Contributes to a Pole-Based Error Correction Pathway. *Curr Biol* 25: 1842–1851

Yen TJ, Compton DA, Wise D, Zinkowski RP, Brinkley BR, Earnshaw WC & Cleveland DW (1991) CENP-E, a novel human centromere-associated protein required for progression from metaphase to anaphase. *EMBO J* 10: 1245–1254

Yen TJ, Li G, Schaar BT, Szilak I & Cleveland DW (1992) CENP-E is a putative kinetochore motor that accumulates just before mitosis. *Nature* 359: 536–539

Yoshizawa K, Matsura A, Shimada M, Ishida-Ishihara S, Sato F, Yamamoto T, Yaguchi K, Kawamoto E, Kuroda T, Matsuo K, *et al* (2023) Tetraploidy-linked sensitization to CENP-E inhibition in human cells. *Mol Oncol* 17: 1148–1166

## MAIN FIGURE LEGENDS

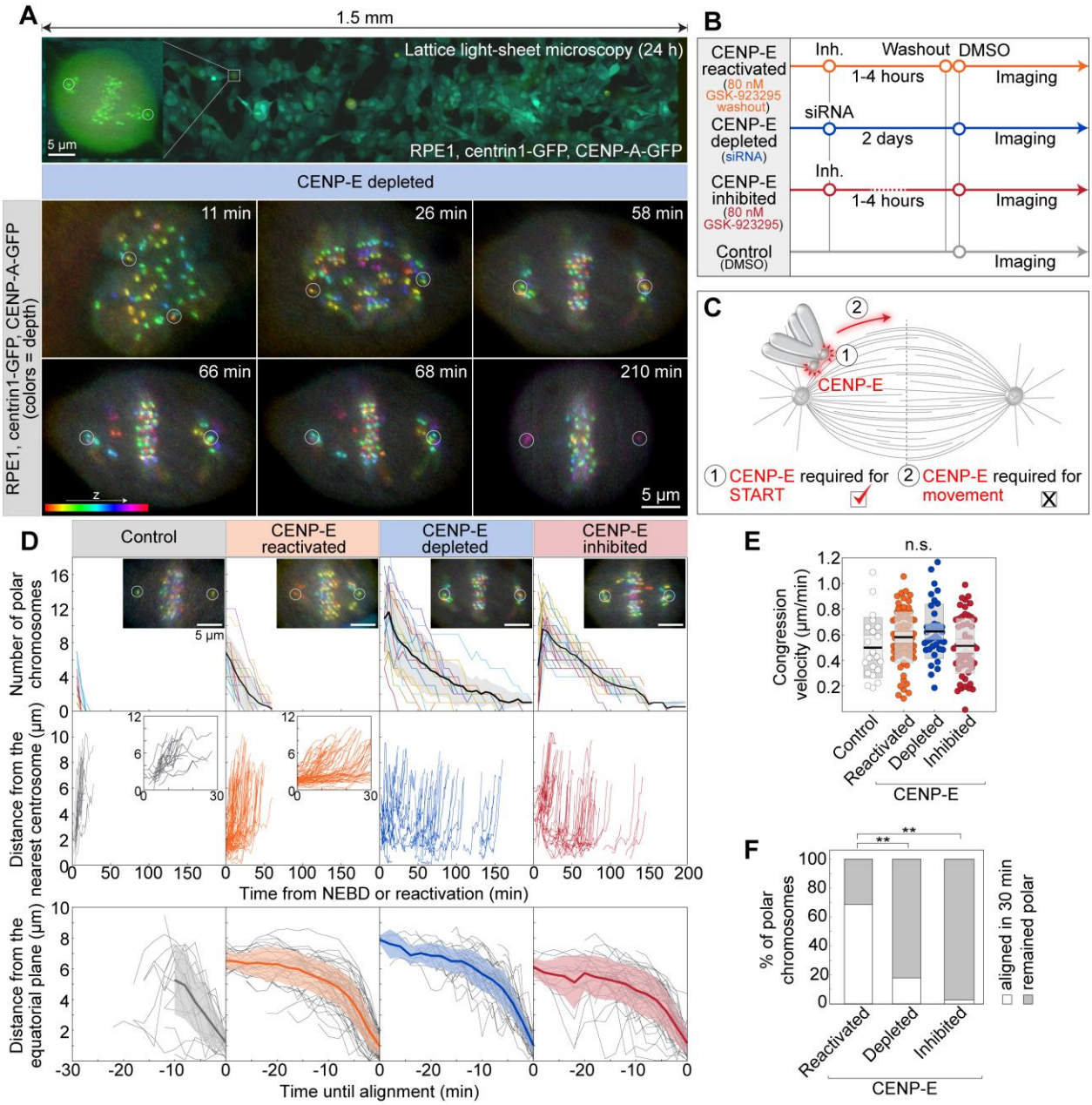


**Figure 1. CENP-E activity is required only for rapid initiation and not for the movement of polar chromosomes during congression.** (A) Field of imaging is 1.5 mm wide and includes dozens of RPE-1 cells expressing centrin1-GFP and CENPA-GFP imaged by lattice light sheet microscopy (LLSM). Cells were treated with the 80 nM CENP-E inhibitor GSK-923295 for 3 h prior to imaging. The boxed area on the left showcases a zoom in on one of the mitotic cells from the imaged area, with a scale bar of 5 µm (top). Example of a representative RPE-1 cell undergoing mitosis after CENP-E depletion imaged using the same assay (bottom). The images are maximum projections color coded for depth (see color bar). Time 0 represents the onset of mitosis. (B) Scheme of the protocol to obtain varying and acutely controllable levels of CENP-E activity in

cells. (C) Scheme depicting the hypothesis that CENP-E, depicted by red glow signs, is required for the initiation of chromosome congression (START), depicted by 1, or for the movement of chromosomes during congression, depicted by 2. The tick represents the interpretation favored by the obtained results. (D) Number of polar chromosomes in time over different treatments, depicted in different colors (top). Distance from the nearest pole of polar kinetochore pairs in time from nuclear envelope breakdown (NEBD) or washout time for CENP-E reactivated condition, with enlargements of data over the x-axis in the upper right part. The lines represent all kinetochores that were defined as polar 10 minutes after nuclear envelope breakdown and that we were able to discriminate from neighboring kinetochores immediately prior and during congression movement (middle). Distance from the equatorial plane kinetochore pairs over time until alignment in different treatments. Thick lines represent means, and the grey areas over means represent standard deviations (bottom). (E) Velocity of chromosome congression during the 6-minute period that precedes alignment for depicted treatments. The black line shows the mean; the light grey and dark grey areas mark the 95% confidence interval on the mean and standard deviation, respectively. Numbers D and E: control (15 cells, 32 kinetochore pairs), reactivated (18 cells, 86 kinetochore pairs), CENP-E depleted (18 cells, 69 kinetochore pairs), inhibited (12 cells, 65 kinetochore pairs), each from at least three independent biological replicates. (F) Percentage of polar kinetochore pairs that aligned (white) or remained polar (grey) during the 30-minute period from the end of prometaphase spindle elongation in the indicated treatments. Statistics: Tukey's HSD test (n.s., non-significant, $*p < 0.05$; $**p < 0.01$; $***p < 0.001$; $****p < 0.0001$). Inh., inhibitor; siRNA, small interfering RNA.

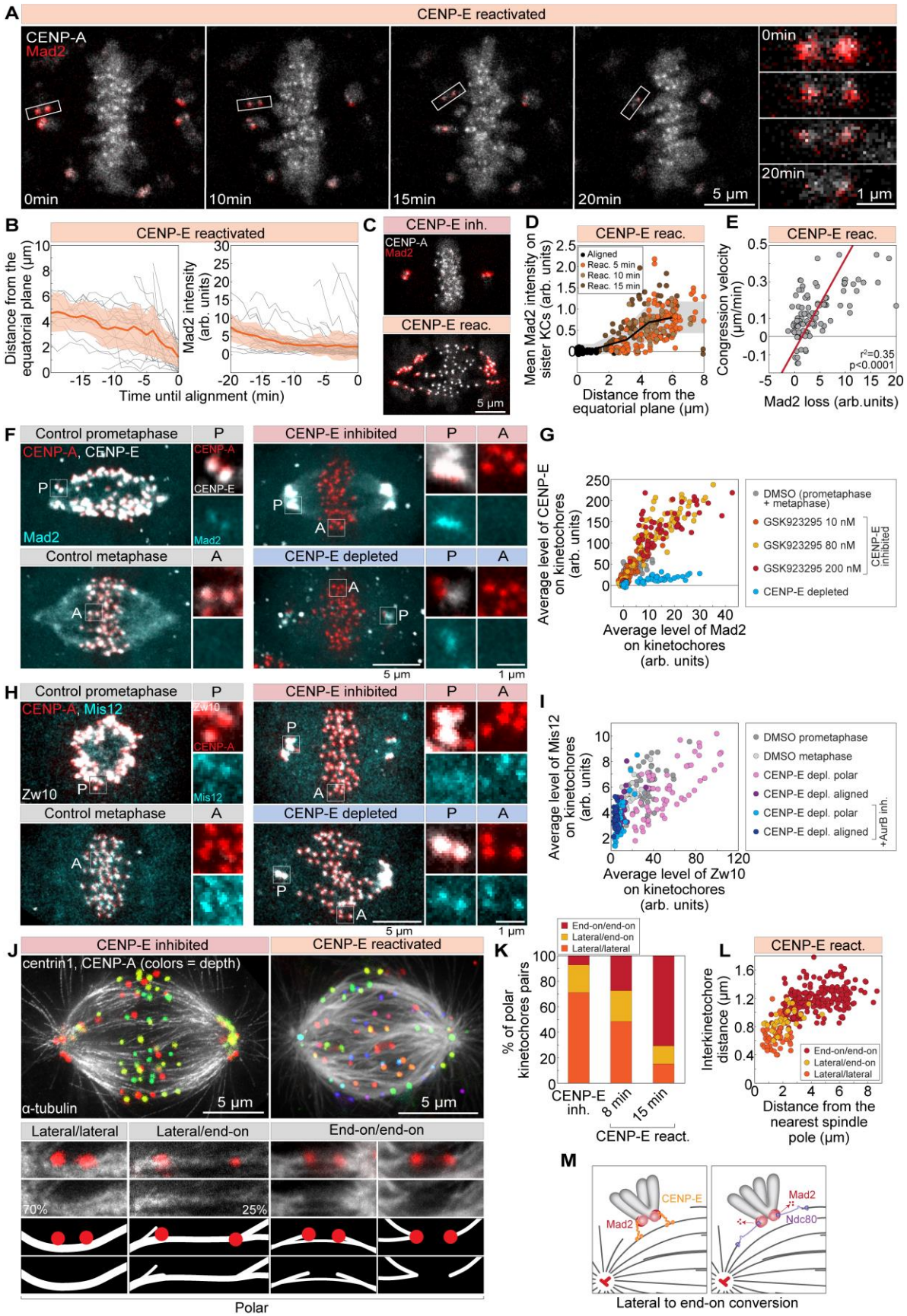
A
CENP-E reactivated
CENP-A
Mad2
0min
10min
15min
20min
5 µm
1 µm
B
CENP-E reactivated
Distance from the equatorial plane (µm)
Mad2 intensity (arb. units)
Time until alignment (min)
C
CENP-E inh.
CENP-A
Mad2
CENP-E reac.
5 µm
D
CENP-E reac.
Aligned
Reac. 5 min
Reac. 10 min
Reac. 15 min
Mean Mad2 intensity on sister KCs (arb. units)
Distance from the equatorial plane (µm)
E
CENP-E reac.
Congression velocity (µm/min)
r²=0.35
p<0.0001
Mad2 loss (arb.units)
F
Control prometaphase
CENP-A, CENP-E
Mad2
CENP-E inhibited
Control metaphase
CENP-E depleted
P
A
5 µm
1 µm
G
Average level of CENP-E on kinetochores (arb. units)
Average level of Mad2 on kinetochores (arb. units)
DMSO (prometaphase + metaphase)
GSK923295 10 nM
GSK923295 80 nM
GSK923295 200 nM
CENP-E depleted
CENP-E inhibited
H
Control prometaphase
CENP-A, Mis12
Zw10
CENP-E inhibited
Control metaphase
CENP-E depleted
5 µm
1 µm
I
Average level of Mis12 on kinetochores (arb. units)
Average level of Zw10 on kinetochores (arb. units)
DMSO prometaphase
DMSO metaphase
CENP-E depl. polar
CENP-E depl. aligned
CENP-E depl. polar
CENP-E depl. aligned
+AurB inh.
J
CENP-E inhibited
CENP-E reactivated
centrin1, CENP-A (colors = depth)
α-tubulin
5 µm
Lateral/lateral
Lateral/end-on
End-on/end-on
70%
25%
Polar
K
End-on/end-on
Lateral/end-on
Lateral/lateral
% of polar kinetochores pairs
CENP-E inh.
8 min
15 min
CENP-E react.
L
CENP-E react.
Interkinetochore distance (µm)
Distance from the nearest spindle pole (µm)
M
CENP-E
Mad2
Ndc80
Lateral to end-on conversion

**Figure 2. Initiation of chromosome congression is accompanied by lateral to end-on transition of microtubule attachments to kinetochores.** (A) Representative example of a cell expressing Mad2-mRuby (red) and CENPA-mCerulean (grey) at different times after the washout of the CENP-E inhibitor as depicted. Images on the right are enlargements of sister kinetochores during congression, as per the boxed area on the left. Time 0 represents the washout of the CENP-E inhibitor. (B) Distance of polar kinetochore from the equatorial plane (left), and mean Mad2 intensity on polar kinetochore pairs (right) in time until alignment. (C) Representative examples of cells expressing Mad2-mRuby (red) and CENPA-mCerulean (grey) fixed in the presence of CENP-E inhibitor (top) or 5 minutes after the washout of the inhibitor (bottom) (left). (D) Distance of polar kinetochore pairs from the metaphase plate over the mean Mad2 signal intensity of kinetochore pairs under indicated conditions. Thick line represents the mean for binned data values, and the grey area over the mean represents the standard deviation of the mean for binned data (right). (E) Congression velocity during the 30-minute period after CENP-E inhibitor washout over the loss of Mad2 signal intensity in kinetochore pairs and linear regression (line). Negative values represent the movement of the kinetochore pair from the metaphase plate. (F-I) Representative examples of cells expressing Mad2-mRuby (cyan) and CENPA-mCerulean (red) immunostained for CENP-E (grey) (F) and cells expressing Mis12-mCherry (cyan) and CENP-A-GFP (red) immunostained for Zw10 (grey) (H) after the indicated treatments. Images are maximum intensity projections of merged channels (left) and enlarged kinetochore pairs per boxed area (right). A, aligned, P, polar. Average level of Mad2 on kinetochores versus average level of CENP-E on kinetochores (G) and average level of Zw10 on kinetochores versus average level of Mis12 on kinetochores (I) in different treatments as per legend on the right. (J) Representative examples of spindles after CENP-E inhibition (left) or 15 minutes after CENP-E reactivation (right) immunostained for α-tubulin and imaged by stimulated emission depletion (STED) microscopy in cells expressing CENP-A-GFP and centrin1-GFP. Projection is color coded by depth as specified by the color bar in 1A (top). Insets of kinetochore pairs with microtubules from different attachment categories, as depicted, and schemes of microtubules (white) and kinetochores (red) of the respective insets (bottom). (K) Percentage of indicated attachment categories across kinetochores per the indicated treatment groups. (L) Distance from the nearest spindle pole of kinetochore pair versus interkinetochore distance in the indicated attachment categories as per legend in the graph. (M) Scheme depicting the model based on obtained results in which CENP-E is essential for rapid lateral-to-end-on conversion close to the spindle pole. All images are a maximum projection of all acquired z planes. Numbers: B, E (14 cells, 54 kinetochore pairs), D (26 cells, 135 kinetochore pairs), G (53 cells, 744 kinetochores), I (57 cells, 666 kinetochores), K and L (69 cells, 380 kinetochore pairs), each from at least three independent biological replicates. Statistics: Tukey's HSD test (n.s., non-significant, $*p < 0.05$; $**p < 0.01$; $***p < 0.001$; $****p < 0.0001$). arb., arbitrary; inh., inhibited; depl, depleted; reac., reactivated.

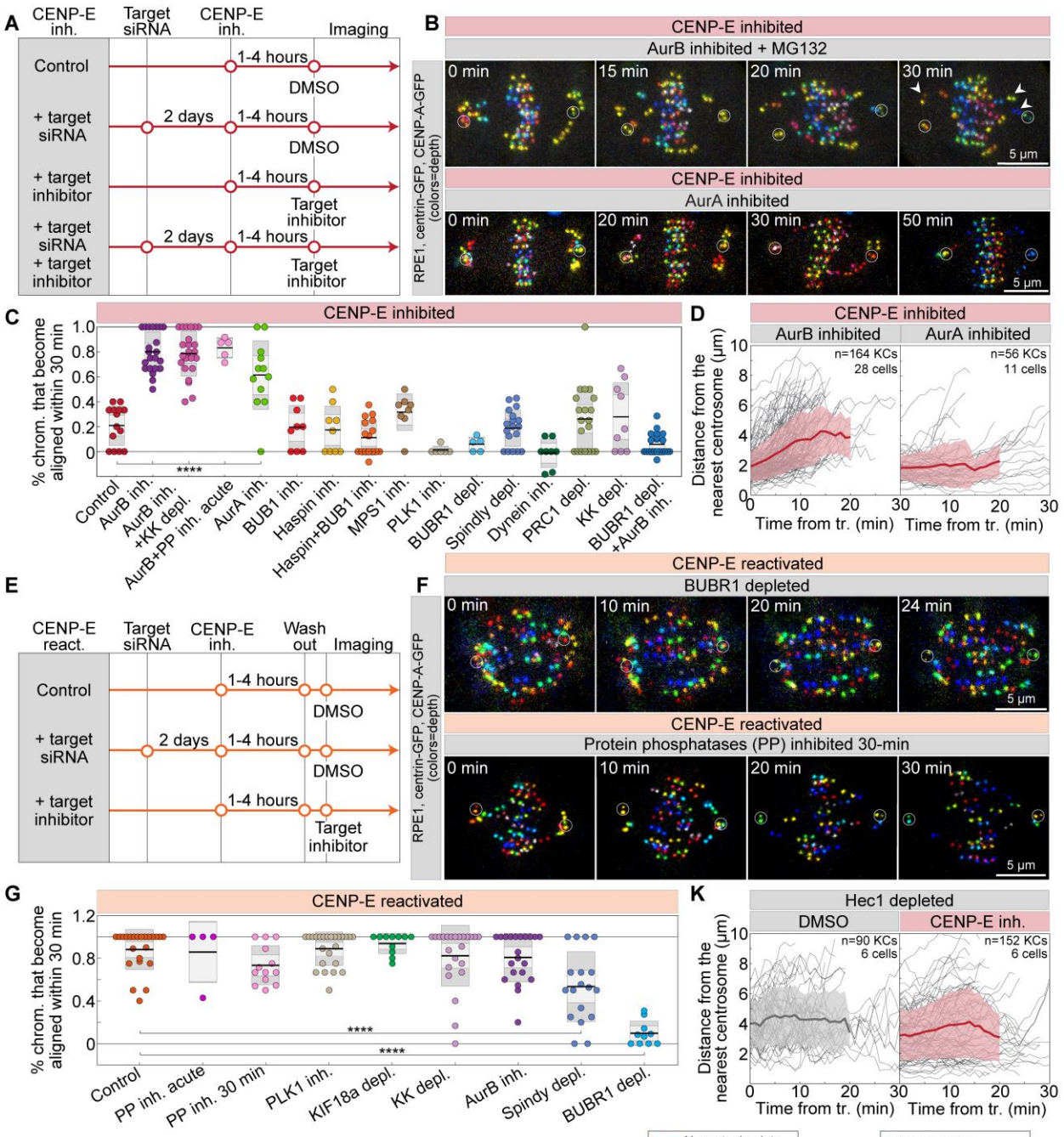
A
CENP-E inh.
Target siRNA
CENP-E inh.
Imaging
Control
1-4 hours
DMSO
+ target siRNA
2 days
1-4 hours
DMSO
+ target inhibitor
1-4 hours
Target inhibitor
+ target siRNA + target inhibitor
2 days
1-4 hours
Target inhibitor
B
CENP-E inhibited
AurB inhibited + MG132
0 min
15 min
20 min
30 min
5 µm
CENP-E inhibited
AurA inhibited
0 min
20 min
30 min
50 min
5 µm
RPE1, centrin-GFP, CENP-A-GFP (colors=depth)
C
CENP-E inhibited
% chrom. that become aligned within 30 min
****
Control
AurB inh.
AurB inh. +KK depl.
AurB+PP inh. acute
AurA inh.
BUB1 inh.
Haspin inh.
Haspin+BUB1 inh.
MPS1 inh.
PLK1 inh.
BUBR1 depl.
Spindly depl.
Dynein inh.
PRC1 depl.
KK depl.
BUBR1 depl. +AurB inh.
D
CENP-E inhibited
AurB inhibited
AurA inhibited
n=164 KCs 28 cells
n=56 KCs 11 cells
Distance from the nearest centrosome (µm)
Time from tr. (min)
Time from tr. (min)
E
CENP-E react.
Target siRNA
CENP-E inh.
Wash out
Imaging
Control
1-4 hours
DMSO
+ target siRNA
2 days
1-4 hours
DMSO
+ target inhibitor
1-4 hours
Target inhibitor
F
CENP-E reactivated
BUBR1 depleted
0 min
10 min
20 min
24 min
5 µm
CENP-E reactivated
Protein phosphatases (PP) inhibited 30-min
0 min
10 min
20 min
30 min
5 µm
RPE1, centrin-GFP, CENP-A-GFP (colors=depth)
G
CENP-E reactivated
% chrom. that become aligned within 30 min
****
****
Control
PP inh. acute
PP inh. 30 min
PLK1 inh.
KIF18a depl.
KK depl.
AurB inh.
Spindy depl.
BUBR1 depl.
K
Hec1 depleted
DMSO
CENP-E inh.
n=90 KCs 6 cells
n=152 KCs 6 cells
Distance from the nearest centrosome (µm)
Time from tr. (min)
Time from tr. (min)
H
Non-targeting
Hec1 depl.
Hec1+ HSET depl.
Hec1+HSET +CENP-E depl.
CENP-A, centrin1
Hec1
Depletion 95%
Depletion 99%
Depletion 99%
5 µm
I
No metaph. plate
High missaligment
Low missaligment
Tight metaph. plate
% of metaphase cells
NT
Hec1 depl.
Hec1+HSET depl.
Hec1+HSET depl. +CENP-E inh.
J
Non-targeting
Hec1/Nuf2 depl.
Hec1/Nuf2+HSET depl.
Maximum spread of chromosomes (µm)
Normalized Hec1 kinetochore levels (arb. units)

**Figure 3. Aurora kinases inhibit congression in the absence of CENP-E, whereas lateral attachments and BubR1 are prerequisites for CENP-E-mediated congression.** (A) Scheme of the experimental protocol to test which molecular factors limit chromosome congression in the absence of CENP-E activity. (B) Representative examples of cells expressing CENP-A-GFP and centrin1-GFP (denoted by white circles) in the presence of CENP-E inhibitor at different times after acute inhibition of target proteins as depicted. Time represents the time from the drug treatment. (C) Percentage of polar chromosomes that become aligned in the 30-minute period after indicated treatments in the presence of CENP-E inhibitor. The black line shows the mean; the light and dark grey areas mark the 95% confidence interval on the mean and standard deviation, respectively. Numbers of cells per treatment: 14, 22, 23, 5, 12, 9, 9, 17, 8, 6, 5, 18, 8, 20, 9, 21, each from at least three independent experiments. Negative % means that more chromosomes were polar 30 minutes after CENP-E inhibition compared at the start of inhibition. (D) Distance to the nearest centrosome of initially polar kinetochore pairs in time from the indicated acute treatment. Thick lines represent means, and gray areas over means represent standard deviations. (E) Scheme of the experimental protocol to test which molecular factors regulate the congression of polar chromosomes after the reactivation of CENP-E activity by the wash-out of the CENP-E inhibitor. (F) Representative examples of cells expressing CENP-A-GFP and centrin1-GFP at different times after acute inhibition of the depicted targets following wash-out of the CENP-E inhibitor. Time represents the time from wash-out. (G) Percentage of polar chromosomes that become aligned in the 30-minute period after the wash-out of the CENP-E inhibitor in the indicated treatments. Numbers of cells per treatment: 23, 4, 13, 24, 11, 23, 21, 18, 10, each from at least three independent biological replicates. (H) Representative examples of cells expressing CENP-A-GFP and centrin1-GFP (grey) immunostained for Hec1 (grey), with circled centrioles, in the treatments indicated on top. (I) Percentage of metaphase cells in the denoted treatments with different extent of chromosome misalignments as per legend on the top. (J) Average Hec1 kinetochore levels normalized to non-targeting group average versus the maximum spread of chromosomes in each cell across different treatments as per legend on the top. Numbers: 31, 27, 24, 33 cells per treatment (I), 97 cells in total (K), each treatment done in at least three independent biological replicates. (K) Distance to the nearest centrosome of initially polar kinetochores in time for the treatments indicated on top. All images are maximum projections color-coded by height as specified on the color bar in 1A except images in H. Statistics: Tukey's HSD test (n.s., non-significant, $*p < 0.05$; $**p < 0.01$; $***p < 0.001$; $****p < 0.0001$). Inh., inhibited; depl., depleted; siRNA, small interfering RNA; arb., arbitrarily; PP, protein phosphatases; KK, Kid and Kif4a; KC, kinetochore; NT, non-targeting; tr., treatment; AurB, Aurora B; AurA, Aurora A.

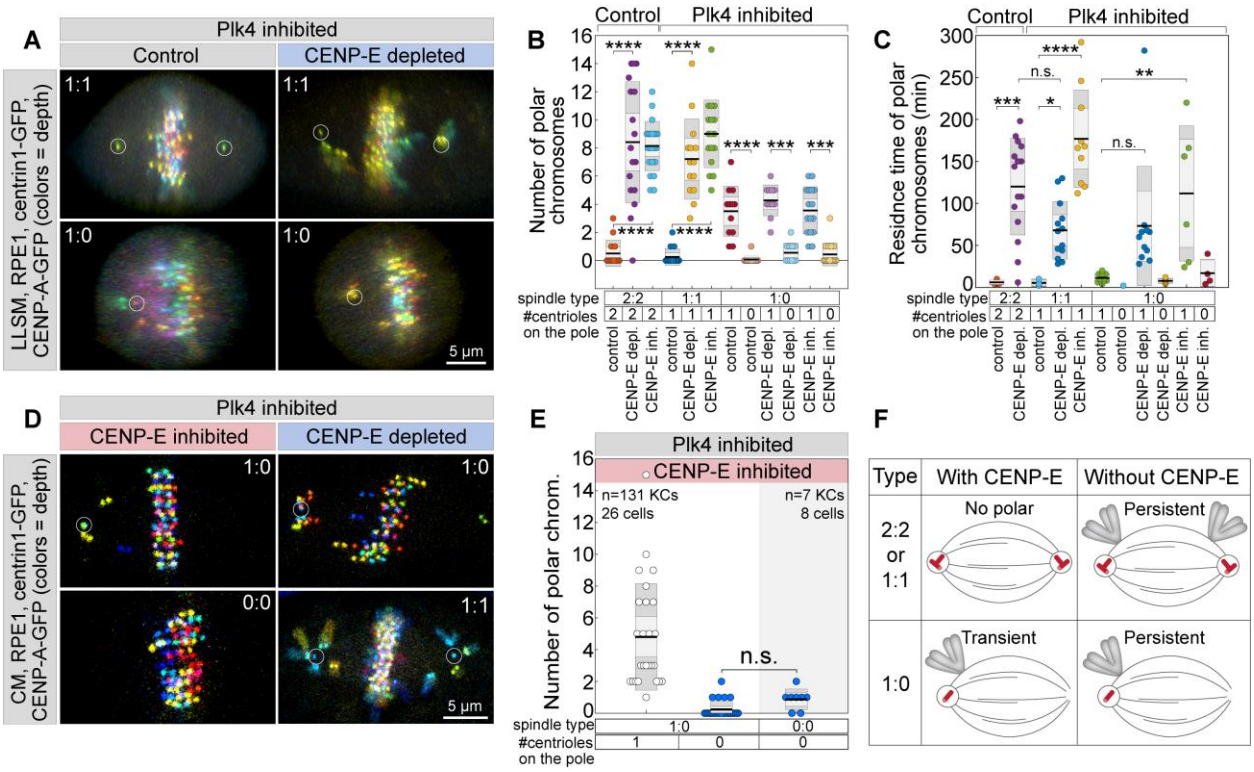


**Figure 4. Centrioles inhibit chromosome congression in the absence of CENP-E activity.** (A) Representative examples of cells expressing CENP-A-GFP and centrin1-GFP with different numbers of centrioles on each pole, which are denoted by white circle, 5 minutes after spindle elongation imaged by lattice light sheet microscopy for treatments indicated on top. (B-C) Number (B) and residence time on spindle pole (C) of polar chromosomes after the end of prometaphase spindle elongation in cells with different numbers of centrioles designated at the bottom across different indicated treatments. The category "1" contains data from centriolar spindle poles from both 1:1 and 1:0 spindles. The black line shows the mean; the light grey and dark grey areas mark the 95% confidence interval on the mean and standard deviation, respectively. Number of cells per condition (B, C): 14, 15, 22, 16, 14, 18, 16, 16, 12, 12, 16, 16, each from at least three independent biological replicates. (D) Representative examples of cells expressing CENP-A-GFP and centrin1-GFP with different numbers of centrioles as indicated. (E) Number of polar chromosomes after different treatments imaged by confocal microscopy in cells with different numbers of centrioles as indicated. Experiment performed in more than three independent biological replicates. (F) Schemes depicting the summary of experimental results for the number and residence time of polar chromosomes on spindle poles for cells characterized by different numbers of centrioles with or without CENP-E activity. All images are maximum projections color-coded by height as specified on the color bar in 1A. Statistics: Tukey's HSD test (n.s., non-significant, $*p < 0.05$; $**p < 0.01$; $***p < 0.001$; $****p < 0.0001$). LLSM, lattice light sheet microscopy; CM, confocal microscopy. inh., inhibited; depl., depleted; chrom., chromosomes; KC, kinetochore.

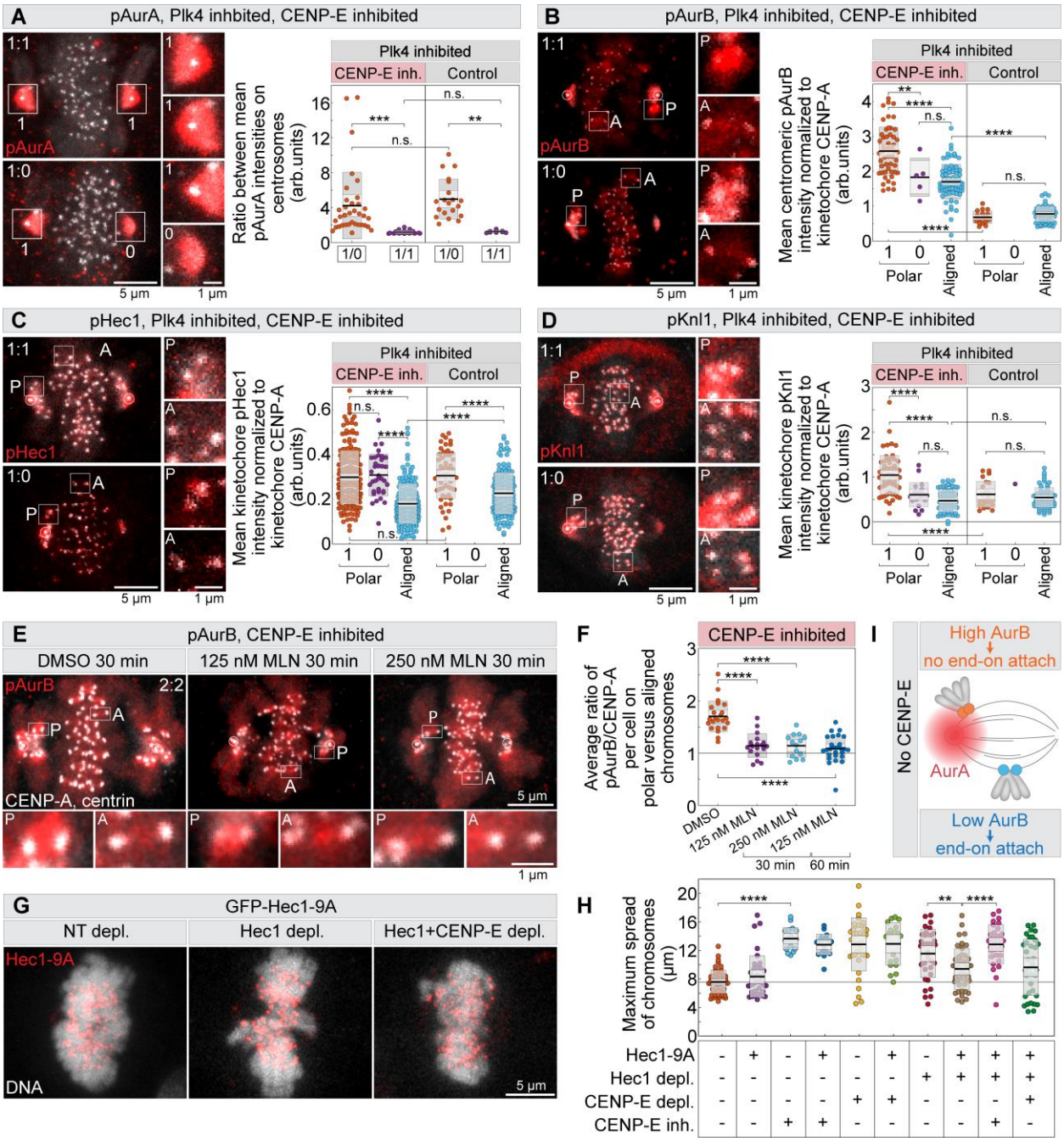


**Figure 5. CENP-E negatively regulates Aurora B kinase activity and its downstream phosphorylation of outer-kinetochore proteins near the centriolar Aurora A gradient.** (A-D) Representative examples of cells expressing CENP-A-GFP and centrin1-GFP (grey), with centrioles denoted by white circles, immunostained with antibodies targeting phosphorylated (p) residues of indicated proteins (red) (pT288-Aurora A, pT232-Aurora B, pS55-Hec1, and pS24, pS60-Knl1) with different numbers of centrioles on each pole as depicted, after treatments as indicated on top, and with enlarged insets of boxed areas on the right. The images are maximum projections (left). P, polar. A, aligned. Ratio between the mean phosphorylated Aurora A in the centriolar spindle pole ("1") versus the acentriolar pole ("0") for the indicated treatments (A), the

mean intensity of the targeted phosphorylated residues in the kinetochore as indicated and normalized to the kinetochore CENP-A intensity for the indicated kinetochore subpopulations and treatments (B-D) (right). Numbers: 88 cells (A), 179 kinetochores from 42 cells (B), 594 kinetochores from 67 cells (C), 227 kinetochores from 63 cells (D), all done in at least two independent biological replicates. (E) Representative examples of cells expressing CENP-A-GFP and centrin1-GFP (grey), with centrioles denoted by white circles, after treatments as indicated on top, and with enlarged insets of boxed areas. Cells were immunostained with antibodies targeting pT232-Aurora B (red). (F) The average ratio of mean intensities of pT232-Aurora B normalized to CENP-A on polar versus on aligned kinetochores per each cell in the indicated treatments. MLN, MLN8237. (G) Representative examples of HeLa cells expressing GFP-Hec1-9A (red) with DNA stained by DAPI (grey) in treatments indicated on the top. (H) Maximum spread of chromosomes in the indicated treatments, as per the legend on the bottom. Numbers: 571 kinetochore pairs from 91 cells (F), 327 cells (H), all done in at least two independent biological replicates. (I) Scheme depicting the model based on experimental results in which the Aurora A activity gradient on centriolar centrosomes upregulates Aurora B activity on kinetochores that limits the establishment of end-on attachments in the absence of CENP-E, while a low level of active Aurora B on kinetochores leads to the establishment of end-on attachments and chromosome congression independently of CENP-E. n.s., nonsignificant. Statistics: Tukey's HSD test (n.s., non-significant, $*p < 0.05$; $**p < 0.01$; $***p < 0.001$; $****p < 0.0001$). Inh., inhibited, depl., depleted, chr., chromosomes; NT, non-targeting; KC, kinetochore.

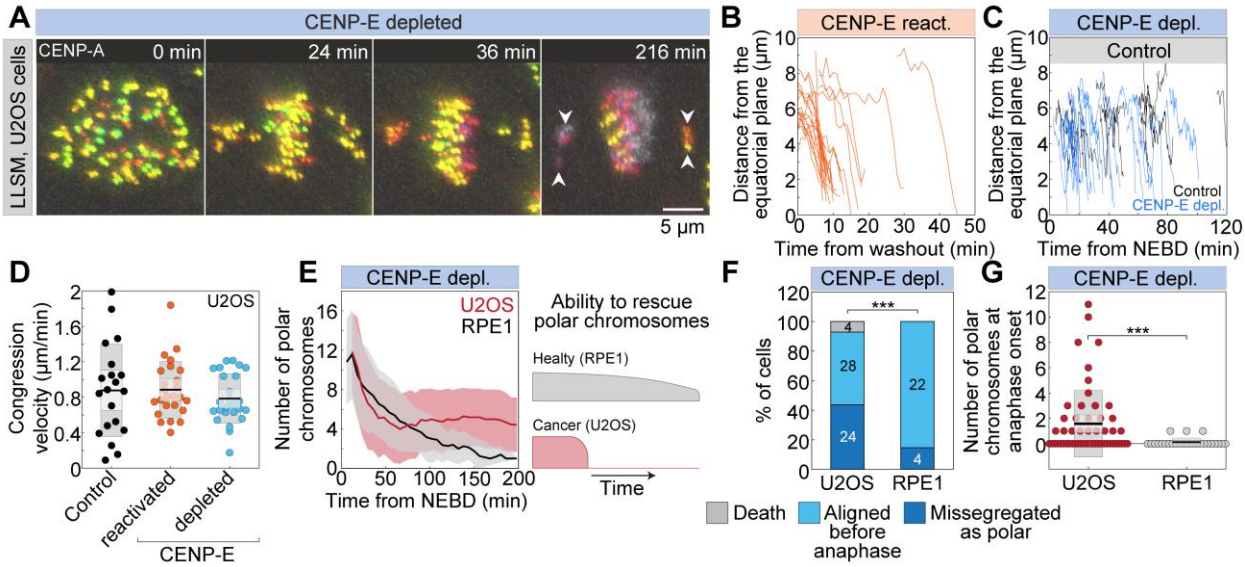


**Figure 6. The congression capacity in U2OS cells is severely reduced in a time-dependent and switch-like manner in the absence of CENP-E.** (A) Example of a representative U2OS cell expressing CENP-A-GFP and undergoing mitosis after depletion of CENP-E. The cell was imaged using the lattice light sheet microscopy (LLSM) assay shown in Figure 1A. Images are maximum projections color coded by height as specified on the color bar in Figure 1A. Time 0 represents the onset of mitosis. Arrowheads depict polar chromosomes in early anaphase. (B, C) Distance from the equatorial plane of initially polar kinetochore pairs in time from washout of the CENP-E

inhibitor (B) or from nuclear envelope breakdown (NEBD) (C). (D) Velocity of chromosome congression during the 4-minute period that precedes complete alignment of polar chromosomes for depicted treatments. The black line shows the mean; the light grey and dark grey areas mark the 95% confidence interval on the mean and standard deviation, respectively. Numbers (B-D): control (30 cells, 64 kinetochore pairs), reactivated (10 cells, 38 kinetochore pairs), depleted (10 cells, 52 kinetochore pairs), each done in at least three independent biological replicates. (E) Number of polar chromosomes in time from NEBD after depletion of CENP-E in RPE-1 (gray) and U2OS (red) cells (left). Scheme showing the ability of given cell line to rescue polar chromosomes in the absence of CENP-E as a function of time inferred from the data presented in the left (right). (F) Percentage of indicated chromosome mis-segregation phenotypes in anaphase cells across depicted cell lines. (G) Number of polar chromosomes at the onset of anaphase across the indicated cell lines. Numbers (E-G): 58 cells (U2OS), 26 cells (RPE-1). Statistics: Tukey's HSD test (n.s., non-significant, $*p < 0.05$; $**p < 0.01$; $***p < 0.001$; $****p < 0.0001$). Depl., depleted; react., reactivated.

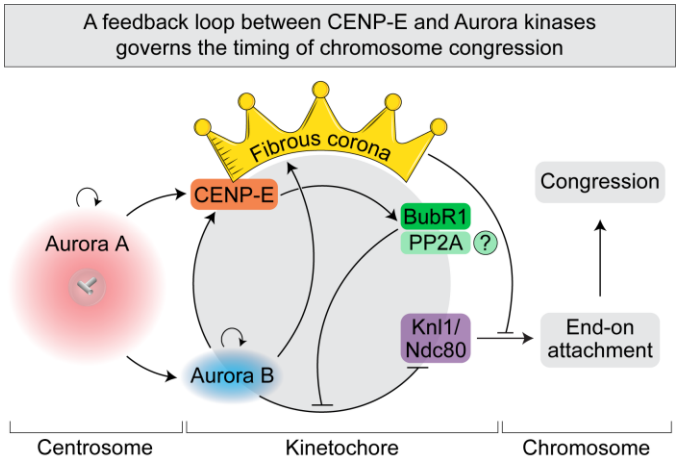


**Figure 7. Model of chromosome congression featuring a negative feedback loop between Aurora B kinase and CENP-E, regulated by the proximity to Aurora A kinase.** Functional negative feedback loop of signaling interactions involving Aurora kinases, CENP-E, BubR1-PP2A, fibrous corona, and outer-kinetochore proteins Knl1/Hec1 (KNL/Ndc80) that governs the formation of end-on attachments and the initiation of chromosome congression. Lines with arrows indicate activation, and blunt lines indicate deactivation. Polar chromosomes initially exhibit lateral attachments of kinetochores to microtubules, which fail to quickly convert to stable end-on attachments without CENP-E due to the high activity of Aurora A (AurA, red gradient centered on centrioles depicted by gray tubules) that activates outer-kinetochore localized Aurora B (AurB), likely by phosphorylation. Activated AurB phosphorylates outer kinetochore proteins like Knl1 and Hec1 (Ndc80), essential for end-on attachment of microtubules to the outer kinetochore, and maintains the expanded fibrous corona (depicted as a crown) that inhibits end-on conversion. Aurora kinases also activate CENP-E by phosphorylation near spindle poles. We propose (?) that the interaction of activated CENP-E with BubR1 and protein phosphatase 2A (PP2A) is required to counteract Aurora B-mediated phosphorylation of outer kinetochore substrates. This stabilizes

initial end-on attachments, initiating gradual end-on conversion and leading to subsequent congression movement of the chromosome towards the spindle midplane.

## EXTENDED VIEW FIGURE LEGENDS

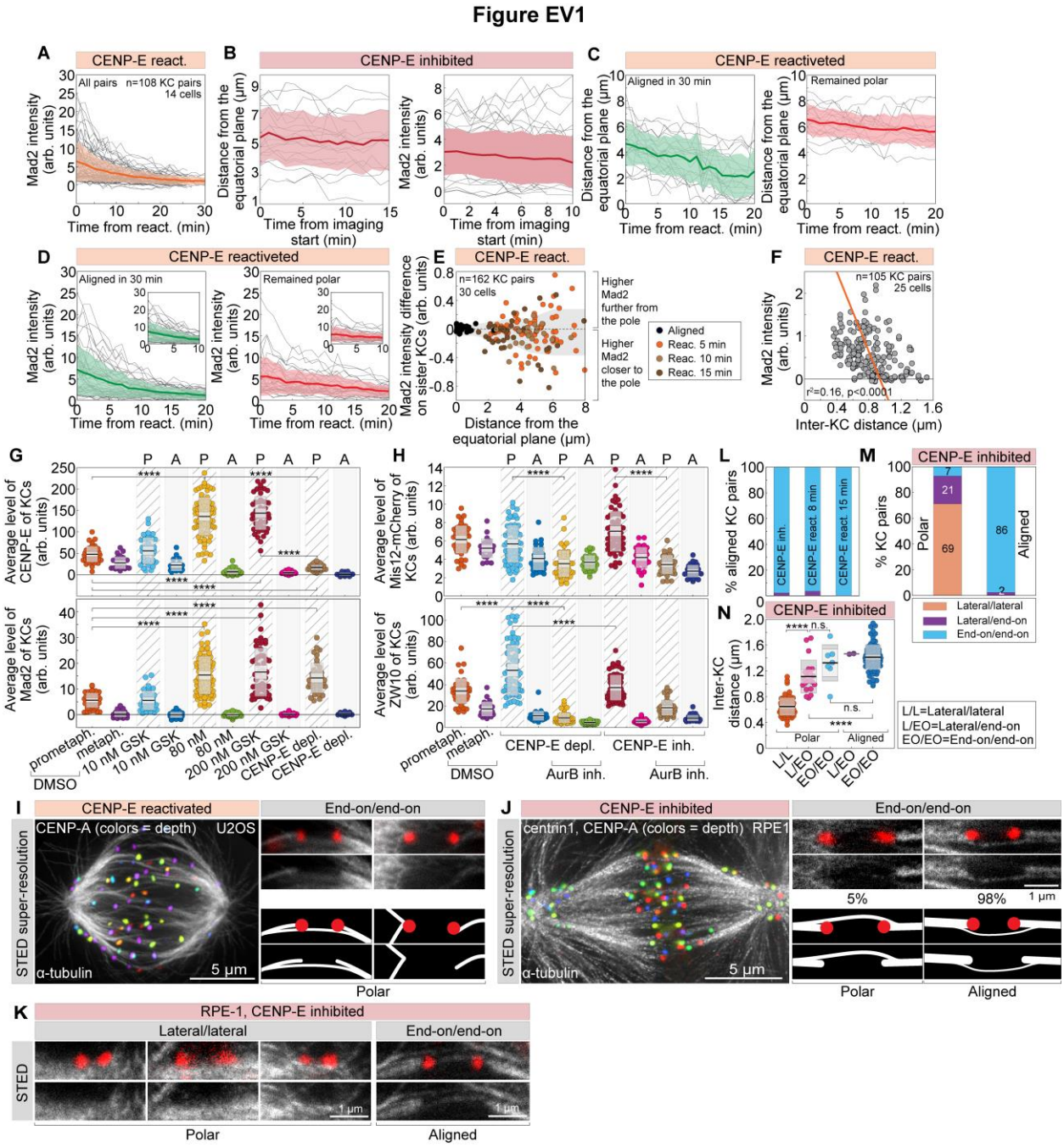


**Figure EV1. In response to CENP-E reactivation Mad2 signal on polar kinetochores gradually drops over time prior to the start of chromosome movement, related to Figure 2.** (A) Mean Mad2 signal intensity of initially polar sister kinetochore pairs over time from the washout of the CENP-E inhibitor. The thick black line represents the mean, and the purple area around the mean represents the standard deviation. (B) Distance of polar kinetochore pairs from the equatorial plane (left) and mean Mad2 signal intensity (right) of polar sister kinetochore pairs over time in the presence of the CENP-E inhibitor. (C, D) Distance from the equatorial plane (C),

and mean Mad2 signal intensity (D) of polar kinetochore pairs over time from the washout of the CENP-E inhibitor for kinetochore pairs that aligned in the 30-minute period (green, left parts) and pairs that did not align in the same period (red, right parts). (E) Distance of kinetochore pairs from the equatorial plane versus difference in Mad2 levels between two sister kinetochores based on proximity of each kinetochore in a pair to the nearest pole under conditions depicted on the right. (F) Interkinetochore (Inter-KC) distance of sister kinetochore pairs versus mean Mad2 signal intensity of sister kinetochore pairs with linear regression (line). (G, H) Mean levels of CENP-E (G, top), Mad2-mRuby (G, bottom), Mis12-Mcherry (H, top), and Zw10 (H, bottom) on kinetochores under the indicated treatments. P, polar; A, aligned. (I, J) Representative examples of U2OS spindle 8 minutes after CENP-E reactivation (left) or RPE-1 spindle after CENP-E inhibition (right), immunostained for α-tubulin and imaged by stimulated emission depletion (STED) microscopy in cells expressing CENP-A-GFP (U2OS) or CENP-A-GFP and centrin1-GFP (RPE-1). Maximum intensity projection is color-coded by depth as specified by the color bar in Figure 1A (top). Insets of kinetochore pairs with microtubules from different attachment categories, as depicted, and schemes of microtubules (white) and kinetochores (red) of the respective insets (bottom). (K) Insets of kinetochore pairs with microtubules from different attachment categories after CENP-E inhibition, as depicted, imaged by STED microscopy (top), and schemes of microtubules (white) and kinetochores (red) of the respective insets (bottom). (L) Percentage of indicated attachment categories over all kinetochore pairs in the indicated groups. (M) Percentage of designated attachment categories over all kinetochore pairs in the indicated groups. (N) Interkinetochore distances for indicated microtubule attachment categories across spindles treated with the CENP-E inhibitor. The black line shows the mean; the light and dark gray areas mark the 95% confidence intervals on the mean and standard deviation, respectively. Numbers not given elsewhere: 28 kinetochore pairs from 10 cells (B), 185 kinetochore pairs from 20 cells (M and N), each from at least two independent biological replicates. Statistics: Tukey's HSD test. KC, kinetochore; inh., inhibited; reac., reactivated; arb., arbitrarily.

**Figure EV2**

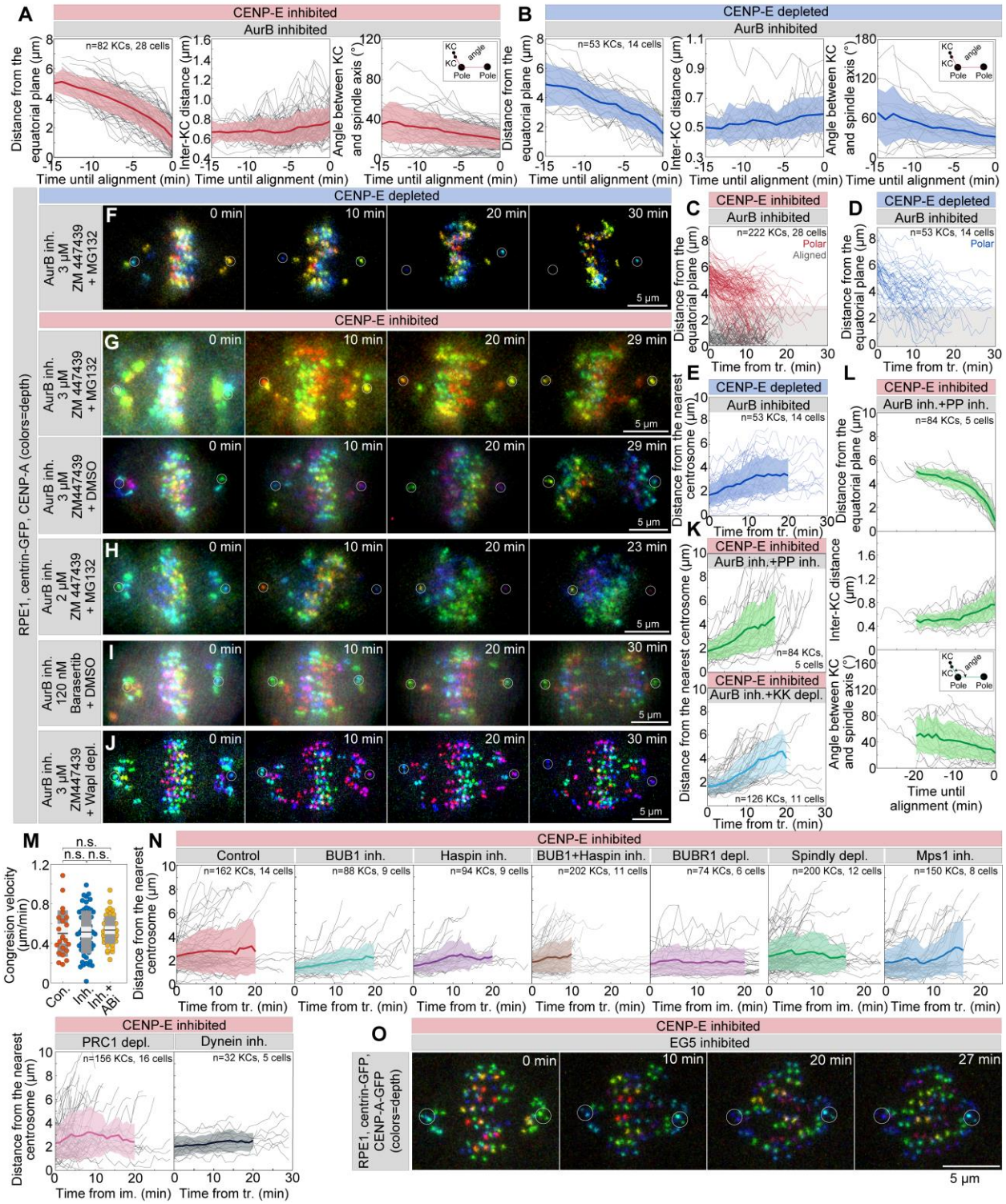


**Figure EV2. Chromosome congression in the absence of CENP-E is limited mainly by the activity of outer-kinetochore pool of Aurora B, related to Figure 3.** (A, B) Distance to the equatorial plane of polar kinetochore pairs (left), interkinetochore (inter-KC) distance (middle),

and angle between sister kinetochores and the main spindle axis as depicted in the scheme at the top (right) over time until alignment of kinetochore pairs after Aurora B acute inhibition by 3 µM ZM447439 in the CENP-E inhibited (A) or depleted (B) cells. Thick lines represent means, and grey areas around the means represent standard deviations. Centrioles are rounded by white circles. (C, D) Distance to the equatorial plane of initially polar (red and blue) and initially aligned (black) sister kinetochore pairs over time from acute addition of 3 µM Aurora B inhibitor ZM447439 in CENP-E inhibited (C) and depleted (D) cells, as indicated. (E) Distance to the nearest spindle pole of initially polar kinetochore pairs (blue) over time from acute addition of 3 µM Aurora B inhibitor ZM447439 in CENP-E depleted cells. (F-J) Representative examples of RPE1 cells expressing CENP-A-GFP and centrin1-GFP in different frames following: acute Aurora B inhibition by 3 µM ZM447439 in cells depleted of CENP-E (F), acute Aurora B inhibition by 3 µM ZM447439 in cells pretreated with CENP-E inhibitor with (G, top) and without (G, bottom) addition of the 20 µM proteasome inhibitor MG132, acute Aurora B inhibition by 2 µM ZM447439 and MG132 in cells pretreated with CENP-E inhibitor (H), acute Aurora B inhibition by 120 nM Barasertib and DMSO in cells pretreated with CENP-E inhibitor (I), and acute Aurora B inhibition by 3 µM ZM447439 and DMSO in cells depleted for 48h of WAPL and treated with CENP-E inhibitor (J). Images are maximum projections color-coded by depth as specified by the color bar in Figure 1A. Centrioles are rounded by the white circles. (K) Distance to the nearest centrosome of initially polar kinetochore pairs over time from the treatments indicated at the top of each graph. (L) Distance to the equatorial plane of initially polar kinetochore pairs (top), interkinetochore (inter-KC) distance (middle), and angle between sister kinetochores and the main spindle axis as depicted in the scheme at the top (bottom) over time until alignment of kinetochore pairs in cells where both Aurora B by 3 µM ZM447439 and protein phosphatases by 1 µM Okadaic acid were acutely inhibited in the CENP-E inhibited cells. (M) Velocity of chromosome congression during the 6-minute period that precedes complete alignment for control (Con), CENP-E inhibited (Inh.) and CENP-E and Aurora B co-inhibited cells (Inh.+Abi). (N) Distance to the nearest centrosome of initially polar kinetochore pairs over time from respective treatments indicated at the top of each graph. (O) Representative example of an RPE1 cell expressing CENP-A-GFP and centrin1-GFP in different frames as depicted after acute addition of 100 µM Eg5 inhibitor Monastrol in the CENP-E inhibited cell. Time represents the time from the acute treatment. Numbers not given elsewhere: 48 kinetochore pairs from 20 cells in M for CENP-E inhibition and Aurora B inhibition, else as in Figure 1. Statistics: Tukey's HSD test. KC, kinetochore; depl., depletion; inh., inhibitited; react., reactivated; tr, treatment; im, imaging; Con., control; AurB, Aurora B; ABi, Aurora B inhibition.

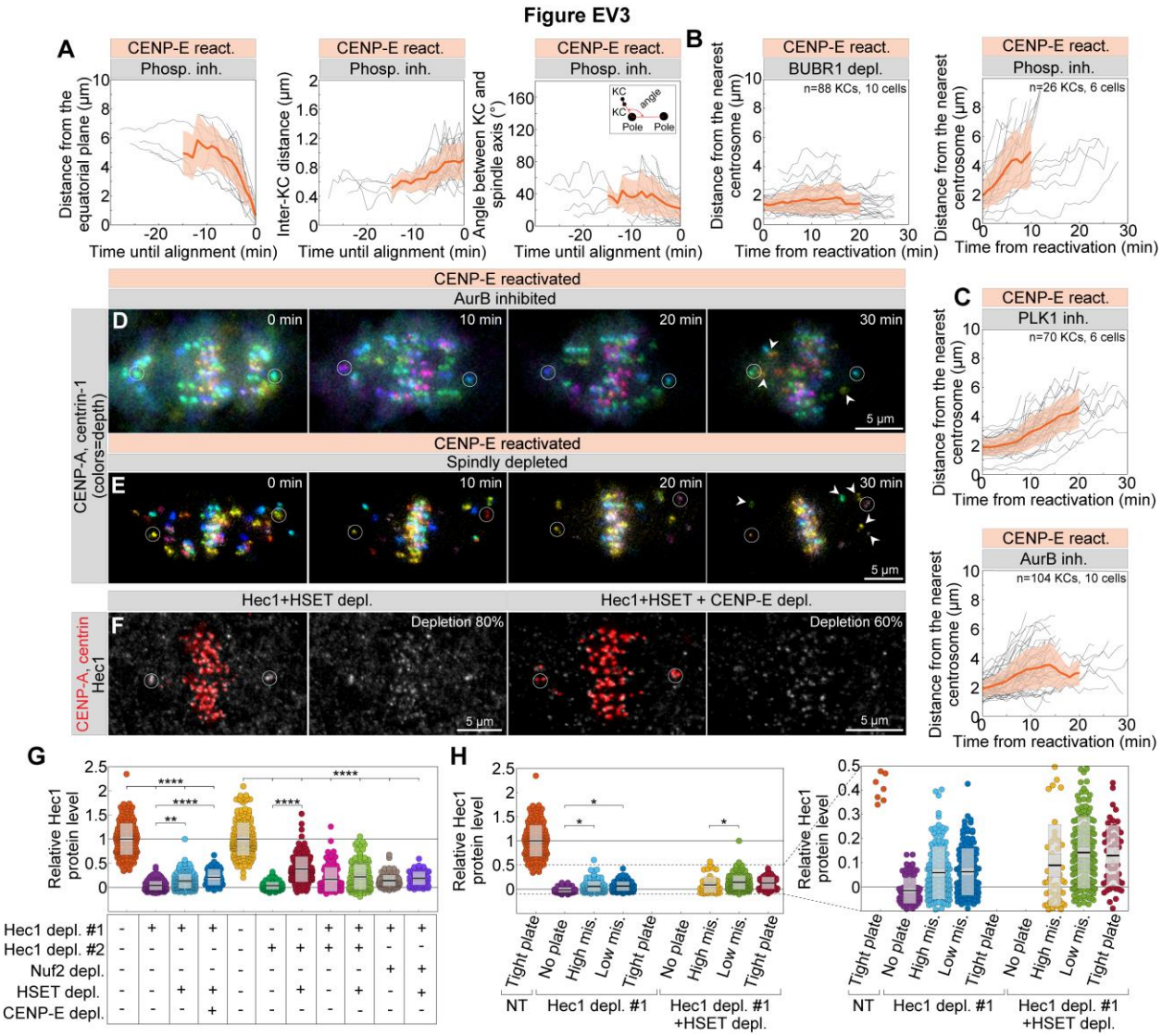


**Figure EV3. Chromosome congression after reactivation of CENP-E activity does not depend on the activity of protein phosphatases, related to Figure 3.** (A) Distance to the equatorial plane of the initially polar kinetochore pairs (left), distance between sister kinetochores (middle), and the angle between sister kinetochores and the main spindle axis, as depicted in the scheme at the top (right), over time until alignment of the kinetochore pair in cells in which protein phosphatases were acutely inhibited by 1 µM Okadaic acid treatment after washout of the CENP-E inhibitor. Thick lines represent means, and grey areas around the means represent standard deviations. (B-C) Distance to the nearest centrosome of initially polar kinetochore pairs over time from the treatment indicated at the top of each graph. (D-E) Representative examples of RPE1 cells expressing CENP-A-GFP and centrin1-GFP in different frames as depicted after washout of the CENP-E inhibitor and addition of 3 µM Aurora B inhibitor ZM447439 (D) or washout of the CENP-E inhibitor in cells depleted of Spindly (E). Images are maximum projections color-coded by depth as specified by the color bar in Figure 1A. Time represents the time from the onset of acute treatment. (F) Representative examples of cells expressing CENP-A-GFP and centrin1-GFP

(denoted by the white circle) and immunostained for Hec1 under the treatments indicated at the top. (G-H) Average level of Hec1 on kinetochores normalized to the average of the non-targeting group over treatments (G) and over treatments and different alignment categories together (H, left) as indicated at the bottom. The graph in H on the right represents the same graph from H on the left but with a shortened y-axis as depicted. Numbers not given elsewhere: 1668 kinetochores from 153 cells (G), 733 kinetochores from 64 cells (H), all from at least three independent biological replicates. Statistics: Tukey's HSD test. KC, kinetochore; inh., inhibited; depl., depleted; AurB, Aurora B; wash., washout; mis., misalignment.

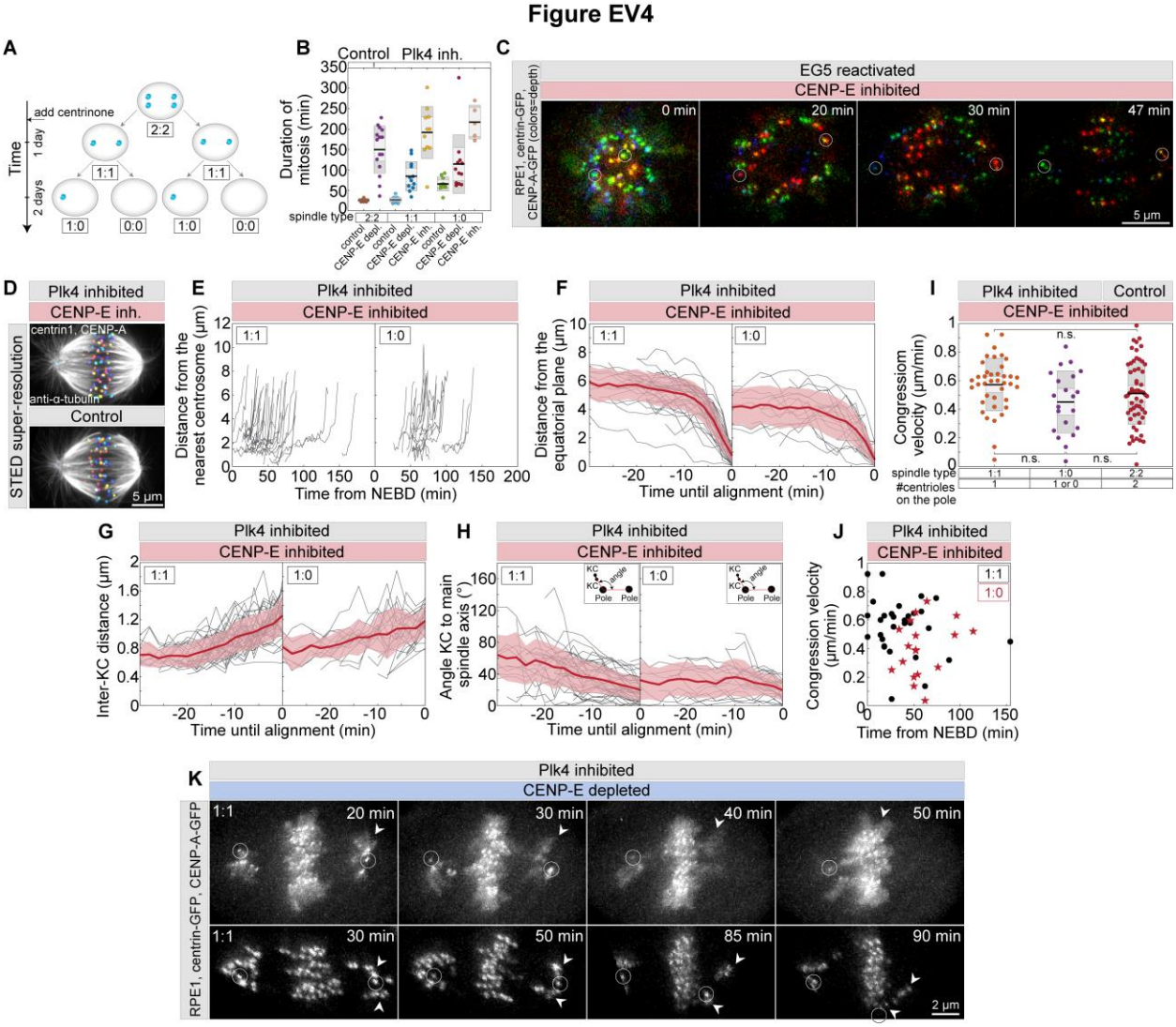


**Figure EV4. Chromosome movement during congression is similar in cells with different numbers of centrioles, related to Figure 4.** (A) Scheme depicting progressive centriole depletion in mitotic cells following continuous Plk4 inhibition by 300 nM centrinone. (B) Duration of mitosis in cells with different numbers of centrioles after treatments indicated at the bottom. The black line shows the mean; the light grey and dark grey areas mark the 95% confidence interval on the mean and standard deviation, respectively. (C) Representative example of an RPE1 cell expressing CENP-A-GFP and centrin1-GFP in different frames from the washout of the Eg5

inhibitor monastrol and acute inhibition of CENP-E by 80 nM GSK923295. Time 0 represents the time of the washout of monastrol and the addition of GSK923295. (D) Representative examples of RPE-1 cells after treatments indicated at the top immunostained for α-tubulin and imaged by stimulated emission depletion (STED) microscopy in cells expressing CENP-A-GFP and centrin1-GFP. Projection is color-coded by depth as specified by the color bar in Figure 1A. (E-H) Distance from the nearest spindle pole over time from nuclear envelope breakdown (NEBD) of initially polar kinetochore pairs (E), distance to the equatorial plane (F), interkinetochore (inter-KC) distance (G), and angle to the main spindle axis depicted in the scheme in the graph (H) of kinetochore pairs over time until alignment for initially polar kinetochores in the presence of the CENP-E inhibitor for cells with different numbers of centrioles as indicated in the top left part of each graph. Thick lines represent means, and pale areas around the means represent standard deviations. (I) Velocity of chromosome congression during the 6-minute period that precedes complete alignment for depicted treatment over time from the onset of mitosis for cells with the number of centrioles as indicated. (J) Velocity of chromosome movement during the 6-minute period that precedes complete alignment versus time from NEBD for each initially polar kinetochore pair. (K) Representative examples of RPE1 cells expressing CENP-A-GFP and centrin1-GFP in different frames from the onset of NEBD after depletion of CENP-E. Centrioles are rounded by the white circle. Arrowheads depict polar chromosomes that align after centriole separation from the centrosome. Statistics: Tukey's HSD test. KC, kinetochore; inh., inhibited; depl., depleted.

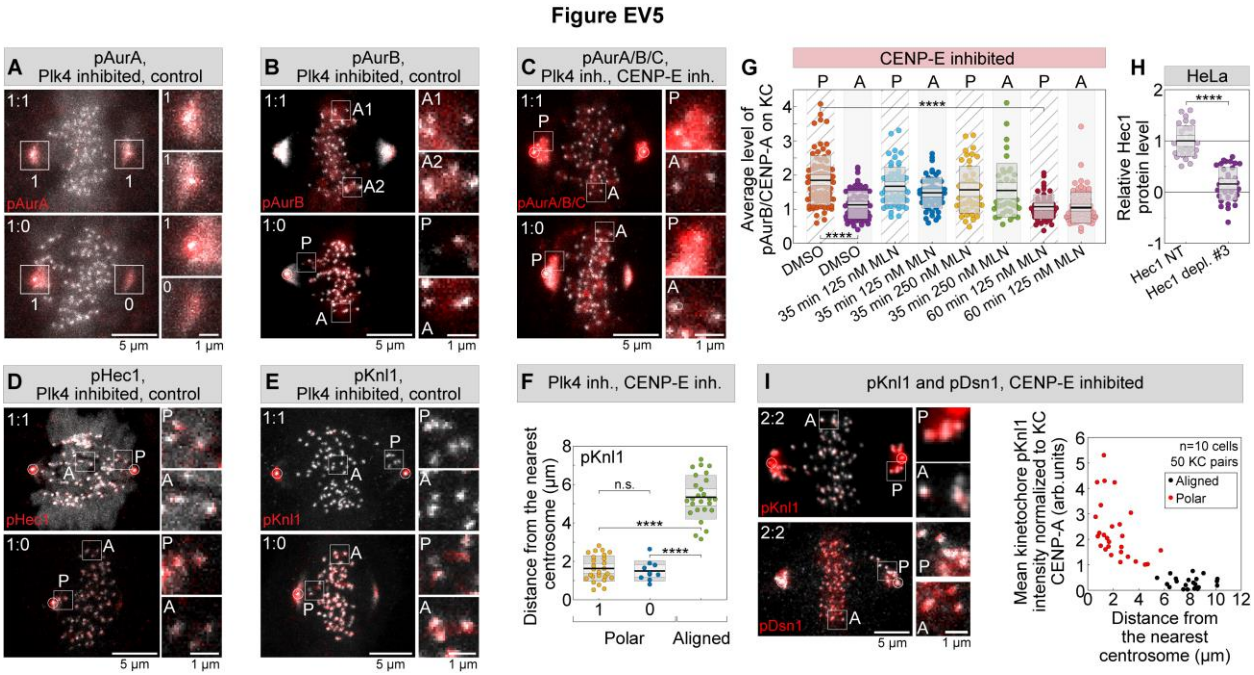


**Figure EV5. Aurora B-mediated phosphorylation declines gradually on outer-kinetochore substrates during congression of polar chromosomes, related to Figure 5.** (A-E) Representative examples (left) and blowups of boxed regions from the left (right) of RPE-1 cells expressing CENP-A-GFP and centrin1-GFP immunostained with antibodies targeting phosphorylated residues of indicated proteins (pT288-Aurora A, pT232-Aurora B, combined

pT288-Aurora A, pT232-Aurora B and pT198-Aurora C, pS55-Hec1, and pS24, pS60-Knl1) with different numbers of centrioles on each spindle pole after 300 nM centrinone treatment and after acute treatment with DMSO (control) as indicated on the top. The images are maximum projections. A, aligned, P, polar. (F) Distance from a spindle pole of different groups of kinetochores as indicated at the bottom from the pKnl1 immunolabelling experiment after acute CENP-E inhibition. (G) Average level of pT232-Aurora B normalized to the average level of CENP-A on kinetochores (KC) after treatments indicated at the bottom. (H) Level of Hec1 measured in DNA area stained by DAPI in HeLa cells normalized to the average level of Hec1 in the non-targeting group (NT) after treatments indicated at the bottom. (I) Representative examples on the left and blowups of boxed regions on the right of RPE-1 cells expressing CENP-A-GFP and centrin1-GFP immunostained with antibodies targeting phosphorylated residues of pKnl1 (top left) and pDsn1 (pS100, pS109-Dsn1, bottom left) after inhibition of CENP-E activity (left) and plot of mean signal intensity of pKnl1 on polar and aligned kinetochore pairs versus the distance of pairs from the spindle pole. n.s., nonsignificant. Numbers not given elsewhere: 65 cells from two independent biological replicates (H). Statistics: Tukey's HSD test. Inh., inhibited; depl., depleted; chr., chromosomes; AurA, Aurora A; AurB, Aurora B; KC, kinetochore.

## APPENDIX FIGURES LEGENDS

### Appendix Figure S1

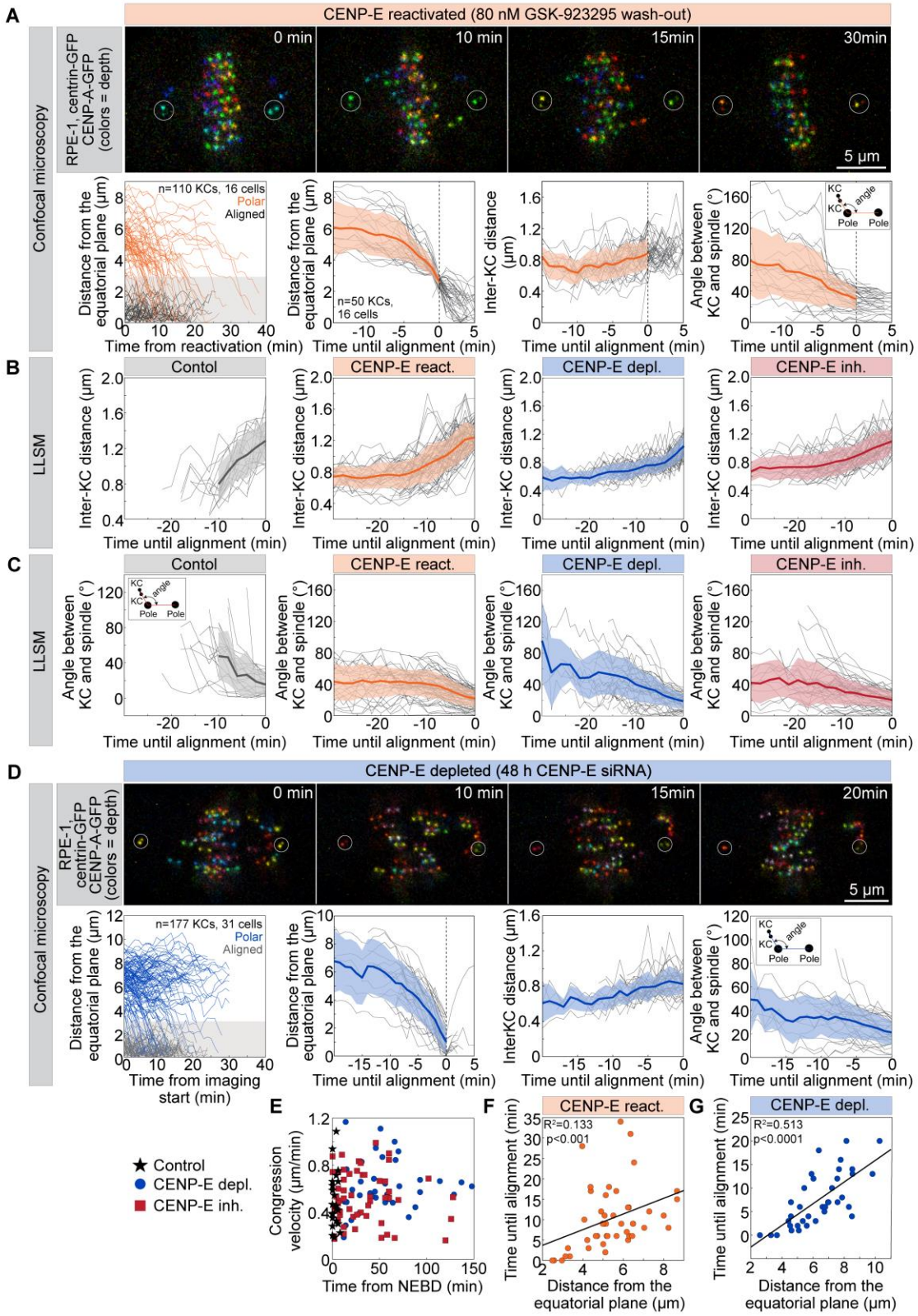

**Appendix Figure S1. Chromosome movement during congression is similar in RPE-1 cells with and without CENP-E activity, related to Figure 1.** (A) Representative example of an RPE1 cell expressing CENP-A-GFP and centrin1-GFP in different frames as depicted after wash-out of the CENP-E inhibitor 80 nM GSK923295 and imaging by confocal microscopy. The image is a maximum projection color-coded by depth as specified by the color bar on Figure 1A (top). Distance from the equatorial plane of sister kinetochores for initially polar (orange lines) and aligned (black lines) kinetochore pairs in time from the washout of the CENP-E inhibitor, distance from the equatorial plane of sister kinetochores for initially polar kinetochore pairs, distance between sister kinetochores (inter-KC), and angle between sister kinetochores and the main spindle axis, as depicted in a scheme in the top-left graph in time until alignment of the kinetochore pair across the indicated treatment. Thick lines represent means, and grey areas over means represent standard deviations (bottom). Centrioles are rounded by the white circle. (B) Distance between polar kinetochores (inter-KC) in time until alignment of the kinetochore pair across indicated treatments for cells imaged by lattice light sheet microscopy (LLSM). (C) Angle between polar kinetochores and the main spindle axis, as depicted in a scheme in the top-left graph in time until alignment of the kinetochore pair across indicated treatments for cells imaged by LLSM. (D) Representative example of an RPE1 cell expressing CENP-A-GFP and centrin1-GFP in different frames as depicted after depletion of CENP-E for 48h and imaged by confocal microscopy. The image is a maximum projection color-coded by depth as specified by the color bar on Figure 1A (top). Distance from the equatorial plane of sister kinetochores for initially polar (blue lines) and aligned (black lines) pairs in time from the washout of the CENP-E inhibitor, distance from the equatorial plane of sister kinetochores for initially polar kinetochore pairs, distance between sister kinetochores (inter-KC), and angle between sister kinetochores and the main spindle axis, as depicted in a scheme in the top-left graph in time until alignment of the kinetochore pair across the indicated treatment. Thick lines represent means, and grey areas over means represent standard deviations (bottom). (E) Congression velocity for polar kinetochore pairs during the last 6 minutes of chromosome congression versus time from nuclear envelope breakdown (NEBD) for treatments indicated in the legend on the left. (F and G) Distance to the equatorial plane of the polar kinetochore pairs versus the time of alignment of each pair in the cells after washing out the CENP-E inhibitor (F) and the depletion of CENP-E (G), where the line represents regression. Statistics: Tukey's HSD test. KC, kinetochore; depl., depleted; inh., inhibited; react., reactivated; NEBD, nuclear envelope breakdown.

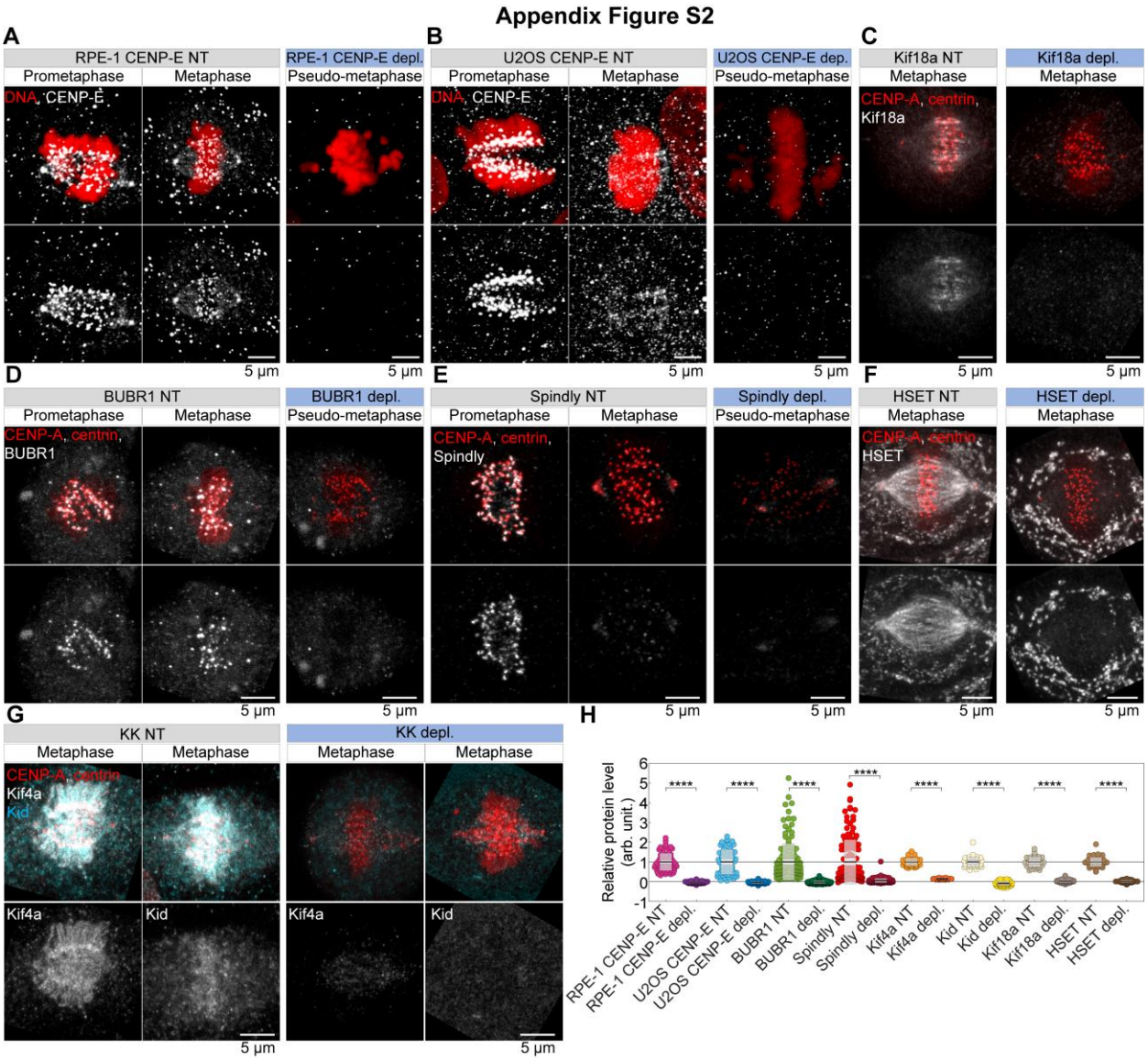


**Appendix Figure S2. Immunofluorescence analysis of RNA interference efficiency for various targets.** (A-G) Representative examples of RPE-1 (A, C-G) and U2OS (B) cells after treatment with non-targeting (NT) small interfering RNAs (siRNAs) and immunofluorescence with antibodies targeting proteins depicted in gray, in different stages of mitosis as labeled (left) and after treatment with targeting siRNAs for different targets as indicated (right). RPE-1 cells were either wild-type (WT) and stained with DAPI (A, red) or expressed CENP-A-GFP and centrin-GFP (C-G, red). U2OS cells were wild-type (WT) and stained with DAPI (B, red). Top images represent maximum projections with merged channels, and bottom images represent only the channel in gray, representing the signal of the antibody targeting the protein that was targeted by the depicted siRNA. (H) Average protein level relative to the average of the non-targeting control group for depicted proteins. Numbers: 70, 66, 56, 53 cells (CENP-E); 137, 116, 121, 144 kinetochores from 14, 13, 15, 15 cells (BubR1 and Spindly); 36, 42, 35, 43, 34, 38, 42 and 36 cells (Kid to HSET), all in at least two independent biological replicates. depl., depletion. Statistics:

Tukey's HSD test (n.s., non-significant, ∗p < 0.05; ∗∗p < 0.01; ∗∗∗p < 0.001; ∗∗∗∗p < 0.0001). NT, non-targeting; depl., depleted; KK, Kid and Kif4a.

**Appendix Figure S3**

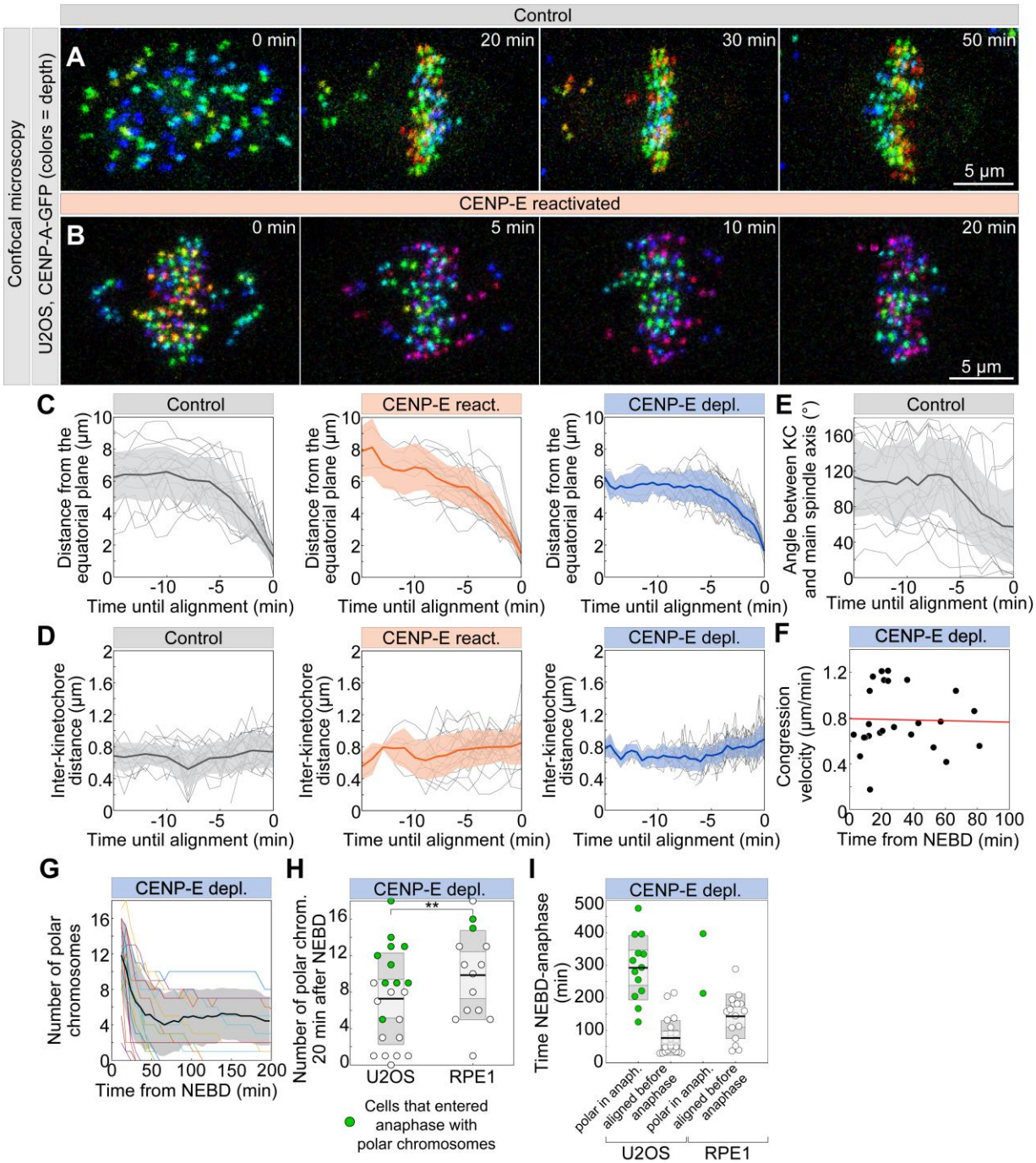


**Appendix Figure S3. Chromosome movement during congression is similar in U2OS cells with and without CENP-E activity, but congression frequently fails in the absence of CENP-E, related to Figure 6.** (A, B) Representative examples of U2OS cells expressing CENP-A-GFP imaged by confocal microscopy in different frames as depicted in control DMSO condition (top)

and after wash-out of the CENP-E inhibitor 200 nM GSK923295. Time 0 represents the onset of nuclear envelope breakdown (NEBD) (A) or wash-out (B). The image is a maximum projection color coded by depth as specified by the color bar on Figure 1A. (C-E) Distance of initially polar kinetochores to the equatorial plate of the spindle (C), interkinetochore (inter-KC) distance (D), and the angle between sister kinetochores and the main spindle axis as depicted on the scheme in the graph (E) in time until alignment of the kinetochore pair across treatments indicated on top of each graph. (F) Velocity of chromosome congression during the last 4 minutes before the polar chromosome aligned to the equatorial plane versus time from from nuclear envelope breakdown (NEBD) for each polar pair and regression (line). (G) Number of polar chromosomes in time from NEBD in U2OS cells after 48h of depletion of CENP-E. Different cells are represented by different colors. Thick lines represent means, and grey areas over means represent standard deviations. (H) Time NEBD to anaphase onset for indicated mitotic outcomes in U2OS and RPE-1 cell lines after CENP-E depletion. The black line shows the mean; the light grey and dark grey areas mark the 95% confidence interval on the mean and standard deviation, respectively. (I) Number of polar chromosomes 20 minutes after NEBD in U2OS and RPE-1 cells depleted of CENP-E. Green squares on (H) and (I) represent cells that eventually entered anaphase with polar chromosomes. Statistics: Tukey's HSD test. depl., depletion, inh., inhibition, react., reactivation.

## EXTENDED VIEW MOVIE LEGENDS

**Movie EV1. Lattice-light sheet microscopy (LLSM)-based assay for large-scale live cell imaging.** Dozens of RPE-1 cells stably expressing CENP-A-GFP and Centrin1-GFP (16-colors) in control cells treated with DMSO, imaged by LLSM right after addition of the drug. Kinetochores and centrioles are color-coded for depth from blue to red with the 16 Colors LUT.

**Movie EV2. RPE1 cells stably expressing CENP-A-GFP and Centrin1-GFP in control and CENP-E reactivated conditions, imaged by LLSM.** RPE-1 cells stably expressing CENP-A-GFP and Centrin1-GFP (16-colors LUT) in cells treated with DMSO (control, left) and after wash-out of the CENP-E inhibitor (CENP-E reactivated, right). Cells were imaged right after the addition of the drug (left) or right after drug wash-out (right). Kinetochores and centrioles are color-coded for depth from blue to red with the 16 Colors LUT.

**Movie EV3. RPE1 cells stably expressing CENP-A-GFP and Centrin1-GFP in CENP-E depleted and CENP-E inhibited conditions, imaged by LLSM.** RPE-1 cells stably expressing CENP-A-GFP and Centrin1-GFP (16-colors LUT) in cells treated with CENP-E siRNA for 48h (CENP-E depleted, left), and with CENP-E inhibitor (CENP-E inhibited, right). Cells were imaged 48h after addition of CENP-E siRNA (left) or 3h after the addition of the CENP-E inhibitor (right). Kinetochores and centrioles are color-coded for depth from blue to red with the 16 Colors LUT.

**Movie EV4. RPE1 cells stably expressing CENP-A-mCerulean and Mad2-mRuby following reactivation of CENP-E activity, imaged by confocal microscopy.** RPE-1 cell stably expressing CENP-A-mCerulean (grey) and Mad2-mRuby (red) in cells treated with CENP-E inhibitor for 3h followed by drug wash-out. Cells were imaged right after wash-out of the drug. Scale bar, 5 µm.

**Movie EV5. RPE1 cells stably expressing CENP-A-GFP and Centrin1-GFP in CENP-E inhibited condition following addition of inhibitors of Aurora kinases, and in CENP-E reactivated condition following depletion of BubR1 and addition of inhibitor of phosphatases, imaged by confocal microscopy.** RPE-1 cells stably expressing CENP-A-GFP and Centrin1-GFP (16-colors LUT) in cells treated with CENP-E inhibitor for 3h followed by acute inhibition of Aurora B kinase (top left), acute inhibition of Aurora A kinase (top right), and in cells treated with CENP-E inhibitor for 3h followed by wash-out of the drug in cells depleted for BubR1 (bottom left), and cells acutely treated by phosphatases inhibitor (bottom right). Cells were imaged right after addition of the last drug or drug wash-out. Kinetochores and centrioles are color-coded for depth from blue to red with the 16 Colors LUT and noise was processed with the Despeckle function in ImageJ.

**Movie EV6. RPE1 cells stably expressing CENP-A-GFP and Centrin1-GFP in Plk4-inhibited cells with different number of centrioles in CENP-E inhibited and CENP-E depleted conditions imaged by confocal microscopy.** RPE-1 cells stably expressing CENP-A-GFP and Centrin1-GFP (16-colors LUT) in cells treated with Plk4 inhibitor for 2 days with distinct number of centrioles on each centrosome (1:1, 1:0, and 0:0) and subsequently treated with CENP-E inhibitor for 3 h before imaging (CENP-E inhibited, left) and with CENP-E siRNA for 48 h before imaging (CENP-E depleted, right). Cells were imaged 48h after addition of CENP-E siRNA (left)

or 3h after the addition of the drug (right). Kinetochores are color-coded for depth from blue to red with the 16 Colors LUT.

**Movie EV7. U2OS cells stably expressing CENP-A-GFP following CENP-E depletion imaged by LLSM.** U2OS cells stably expressing CENP-A-GFP (16-colors LUT) following treatment with CENP-E siRNA for 48h. Cells were imaged 48h after addition of CENP-E siRNA. The noise was processed with the Despeckle function in ImageJ. Kinetochores are color-coded for depth from blue to red with the 16 Colors LUT. Scale bar, 5 µm.